2003-02

Finite Element Analysis of Time-Dependent Semi-Infinite Wave-Guides with High-Order Boundary Treatmen

Neta, Beny

Finite Element Analysis of Time-Dependent Semi-Infinite Wave-Guides with High-Order Boundary Treatment

Dan Givoli * **Beny Neta** †

Department of Mathematics

Naval Postgraduate School

1141 Cunningham Road

Monterey, CA 93943, U.S.A.

Igor Patlashenko ‡

Performance Group, EMC Corporation

171 South Street

Hopkinton, MA 01748-9103, U.S.A.

February 27, 2003

*Corresponding author. E-mail: dgivoli@nps.navy.mil , Tel.: +1-831-656-2758, Fax: +1-831-656-2355. On leave (till Aug. 2002) from: Department of Aerospace Engineering and Asher Center for Space Research, Technion — Israel Institute of Technology, Haifa 32000, Israel, E-mail: givolid@aerodyne.technion.ac.il , Tel.: +972-4-8293814, Fax: +972-4-8231848.

†E-mail: bneta@nps.navy.mil , Tel.: +1-831-656-2235, Fax: +1-831-656-2355.

‡E-mail: igorpt@sympatico.ca .

Abstract

A new Finite Element (FE) scheme is proposed for the solution of time-dependent semi-infinite wave-guide problems, in dispersive or non-dispersive media. The semi-infinite domain is truncated via an artificial boundary $\mathcal{B}$, and a high-order Non-Reflecting Boundary Condition (NRBC), based on the Higdon non-reflecting operators, is developed and applied on $\mathcal{B}$. The new NRBC does not involve any high derivatives beyond second order, but its order of accuracy is as high as one desires. It involves some parameters which are chosen automatically as a pre-process. A C^0 semi-discrete FE formulation incorporating this NRBC is constructed for the problem in the finite domain bounded by $\mathcal{B}$. Augmented and split versions of this FE formulation are proposed. The semi-discrete system of equations is solved by the Newmark time-integration scheme. Numerical examples concerning dispersive waves in a semi-infinite wave guide are used to demonstrate the performance of the new method.

Keywords: Waves, High-order, Artificial boundary, Non-reflecting boundary condition, Finite elements, Higdon, Auxiliary variables, Newmark.

1. Introduction

The numerical solution of exterior wave problems has been an active area of research in the last three decades [1], in the context of various fields of application like acoustics, electromagnetics, meteorology, solid geophysics and aerodynamics. Several types of methods have been developed for such problems. The 70's and early 80's produced some low-order local Non-Reflecting Boundary Conditions (NRBCs) that became well-known, e.g., the Engquist-Majda NRBCs [2] and the Bayliss-Turkel NRBCs [3]. See also the review paper [4]. In addition, the infinite element method was invented [5], and boundary element methods for the solution of infinite-domain problems have become popular; see the historical account by Rizzo [6]. The period between the late 80's and mid 90's has been characterized by the emergence of exact nonlocal NRBCs like those based on the Dirichlet-to-Neumann (DtN) map [7, 8], by the invention of the Perfectly Matched Layer (PML) [9], and by the development of new infinite elements especially designed for wave problems [10, 11]. See, e.g., the special collections of papers on the subject [12]–[14].

The method of NRBCs can be described as follows. First, the infinite domain is truncated via an artificial boundary $\mathcal{B}$, thus dividing the original domain into a finite computational domain Ω and a residual infinite domain D. Then, a special boundary condition is imposed on $\mathcal{B}$, in order to complete the statement of the problem in Ω (i.e., make the solution in Ω unique) and, most importantly, to ensure that no (or little) spurious wave reflection occurs from $\mathcal{B}$. This boundary condition is called a NRBC, although a few other names are often used too [4]. Finally, the problem is solved numerically in Ω, say by the Finite Element (FE) method. The setup is illustrated in Fig. 1.

Fig. 1(a) pertains to an exterior problem outside of a scatterer or an obstacle in full space. The artificial boundary $\mathcal{B}$ has a rectangular shape in the figure, although sometimes a smooth shape (like a circle in two dimensions or a sphere in three dimensions) is preferred. Fig. 1(b) describes a semi-infinite wave-guide problem. In the example shown, $\mathcal{B}$ is a cross section of the wave-guide which constitutes the east side of Ω. In the present paper we shall limit ourselves to the second type of problems, and in particular to two-dimensional semi-infinite wave-guides.

Naturally, the quality of the numerical solution strongly depends on the properties of

the NRBC employed. In the last 25 years or so, much research has been done to develop NRBCs that after discretization lead to a scheme which is stable, accurate, efficient and easy to implement. See [15]–[17] for recent reviews on the subject. Of course, it is difficult to find a single NRBC which is ideal in all respects and all cases; this is why the quest for better NRBCs and their associated discretization schemes continues.

Recently, *high-order* local NRBCs have been introduced. Sequences of increasing-order NRBCs have been available for a long time (e.g., the Bayliss-Turkel conditions [3] constitute such a sequence), but they had been regarded as impractical beyond 2nd or 3rd order from the implementation point of view. Only since the mid 90's, practical high-order NRBCs have been devised. The present paper is concerned with such a high-order NRBC scheme.

The first *high-order* local NRBC has been proposed by Collino [18], for two-dimensional time-dependent waves in rectangular domains. Its construction requires the solution of the one-dimensional wave equation on $\mathcal{B}$. Grote and Keller [19] developed a high-order converging NRBC for the three-dimensional time-dependent wave equation, based on spherical harmonic transformations. Sofronov [20] has independently published a similar scheme in the Russian literature. Hagstrom and Hariharan [21] constructed high-order NRBCs for the two- and three-dimensional time-dependent wave equations based on the analytic series representation for the outgoing solutions of these equations. For time-dependent waves in

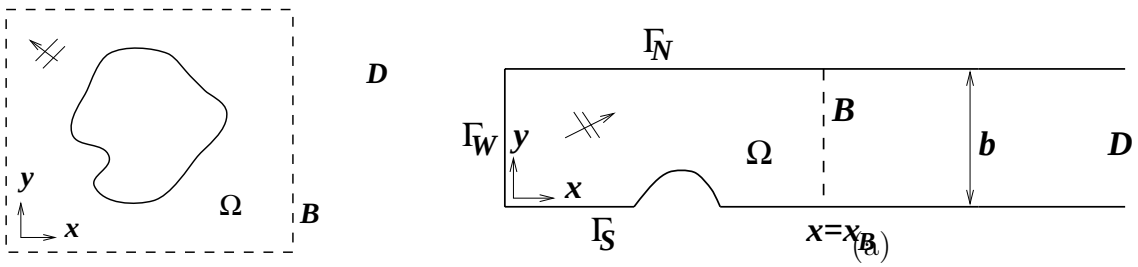

(b)

Figure 1. Setup for the NRBC method: (a) an exterior scattering problem; (b) a semi-infinite wave-guide problem.

a two-dimensional wave guide, Guddati and Tassoulas [22] devised a high-order NRBC by using rational approximations and recursive continued fractions. Givoli [23] has shown how to derive high-order NRBCs for a general class of wave problems, leading to a symmetric FE formulation. In [24], this methodology was applied to the particular case of time-harmonic waves, using optimally localized DtN NRBCs.

In the context of artificial boundary treatment, wave problems can roughly be divided into four categories. These are, in order of difficulty:

(1) Linear time-harmonic wave problems.

(2) Linear time-dependent wave problems in non-dispersive homogeneous media.

(3) Linear time-dependent wave problems in dispersive and/or stratified media.

(4) Nonlinear time-dependent wave problems.

Linear time-harmonic waves have been treated extensively by NRBCs and absorbing layers, including exact NRBCs of the DtN type [16], various PML formulations (see, e.g., [25, 26]), and converging high-order NRBCs (see, e.g., [24]). Time-dependent waves are considerably more difficult to handle from the artificial-boundary perspective. However, some exact and high-order schemes have been devised in this case as well. These include the schemes proposed in the references [18]–[23] mentioned above, as well as a scheme based on the Kirchhoff formula for three-dimensional waves [27, 28], an iterative converging local NRBC [29], semi-discrete DtN [30], time-dependent DtN [31], transform-based methods [32]–[34], and some variations of the above [35]–[37].

The presence of *wave dispersion* and/or medium *stratification* makes the time-dependent problem still more difficult as far as NRBC treatment is concerned. None of the high-order and exact NRBCs mentioned above has been designed to deal with these effects. Very recently, Navon et al. [38] developed a PML scheme for the dispersive shallow water equations. Nonlinear waves (with the nonlinearity extending to infinity) are, of course, the most difficult to handle. Some highly-accurate NRBCs have been proposed for specific classes of nonlinear wave problems (see references in the review papers [15], [17] and [39]).

In this paper, a new family of high-order local NRBCs is developed and incorporated in a FE scheme for the dispersive time-dependent wave equation. Wave dispersion appears in

various applications. One important example is that of rotating systems, like the acoustic medium around helicopter blades, or meteorological models which take into account the earth rotation [40]–[42]. Other examples include the vibration of structures with rotational rigidity such as beams, plates and shells, the vibration of strings and membranes on an elastic foundation, acoustic wave propagation in a bubbly medium, and some nonlinear wave problems after linearization [40].

The starting point for the development of the new family of NRBCs is the NRBC devised by Higdon [43], which was designed for low-order finite difference schemes. In [44], Givoli and Neta extended this formulation in a direct manner to high-order finite difference discretizations. However, the Higdon construction involves spatial and temporal derivatives of increasing orders, and is not compatible with the FE method. In contrast, the NRBCs proposed here, despite being high-order accurate, do not involve any high derivatives beyond second order. The elimination of all high-order derivatives is enabled through the introduction of special auxiliary variables on $\mathcal{B}$. This allows the easy use of the NRBC up to any order desired. The NRBCs involve some parameters which are chosen automatically as a pre-process. A similar construction has been devised in [45] for finite difference schemes. In the present paper, the new NRBCs are incorporated in a standard C^0 FE formulation, which turns out to be stable even with equal-order interpolation for all the variables. The computational effort associated with the high-order boundary scheme will be shown to grow only *linearly* with the order.

Following is the outline of the rest of this paper. In Section 2 the problem under investigation is stated. In Section 3, the new family of high-order NRBCs is developed. In Section 4, a FE semi-discrete formulation is constructed which incorporates a NRBC of this family with any desired order. Two versions of this formulation are presented: a non-symmetric augmented version and a symmetric split version. In Section 5 the Newmark time-integration scheme is applied to the semi-discrete system of equations obtained in the split formulation. In Section 6 some computational issues are discussed. The performance of the method is demonstrated in Section 7 via numerical examples concerning dispersive waves in a semi-infinite wave guide. Some remarks conclude the paper in Section 8.

2. Statement of the Problem

As a model serving for introducing the ideas developed here, wave propagation in a two-dimensional channel or wave guide is considered; see Fig. 1(b). This allows one to concentrate on a single straight artificial boundary (the east boundary $\mathcal{B}$). Extension of the same ideas to other configurations, such as three dimensional wave-guide problems and exterior scattering problems of the type illustrated in Fig. 1(a) with a box-like artificial boundary, is possible. In the latter case, however, the non-trivial issue of *corners* must be dealt with, which is outside the scope of this paper.

The wave guide is assumed to consist of two parts: a finite irregular part Ω and a semi-infinite "uniform tail" D. In the irregular region Ω the geometry, governing equations, and the given initial and boundary conditions are completely general. They are only limited by the capabilities of the finite element code to be used. Thus, the domain Ω may have a general shape (see the "bump" shown in Fig. 1(b)), may include submerged obstacles, and may be associated with inhomogeneity, anisotropy and even nonlinearity. On the other hand, the domain D is assumed to be bounded by two straight parallel rays, and to be associated with none of the irregularities mentioned above. A Cartesian coordinate system (x, y) is introduced such that the wave-guide in D is parallel to the x direction; see Fig. 1(b). The width of the wave-guide in D is denoted by b.

To fix ideas, some specific equations and boundary conditions are chosen here. In Ω, the linear inhomogeneous dispersive (Klein-Gordon) equation is assumed to hold:

$$\ddot{u} - \boldsymbol{\nabla} \cdot C_0^2 \boldsymbol{\nabla} u + f^2 u = S \qquad \text{in} \quad \Omega \ . \tag{1}$$

Here and elsewhere a superposed dot indicates differentiation with respect to time. In (1), u is the unknown wave field, C_0 is the given medium wave speed, f is the given dispersion parameter, and S is a given wave source function. The C_0 and f are functions of location, and the wave source S is a function of location and time. Eq. (1) describes, for example, the lateral vibration of a membrane strip on an elastic foundation, or the acoustic pressure in a dispersive medium (say, a linearized bubbly medium). Also, it can be shown that the linearized (around zero mean flow) shallow water equations with a flat bottom reduce to (1), where u is the water elevation above the reference level [41]. In the geophysical context, f is

called the Coriolis parameter and is related to the angular velocity of the earth. Of course, the method proposed in this paper is also applicable to the case $f = 0$, where (1) becomes the standard scalar wave equation.

In D, the governing equation is a simplified version of (1). It is assumed that in D there are no wave sources (i.e., $S = 0$) and that the coefficients C_0 and f are constants. Thus, eq. (1) becomes

$$\ddot{u} - C_0^2 \, \nabla^2 u + f^2 \, u = 0 \qquad \text{in} \quad D \; . \tag{2}$$

On the south and north boundaries Γ_S and Γ_N, the Neumann condition

$$\frac{\partial u}{\partial \nu} = 0 \qquad \text{on} \quad \Gamma_S \quad \& \quad \Gamma_N \tag{3}$$

is imposed, where $\partial/\partial\nu$ is the normal derivative. In acoustics, (3) corresponds to a "hard wall" condition. On the west boundary Γ_W, u is prescribed, i.e.,

$$u = u_W \qquad \text{on} \quad \Gamma_W \; , \tag{4}$$

where u_W is a given function on Γ_W (incoming wave). It is assumed that no physical boundaries additional to the above (say, of a submerged obstacle) are present. At $x \to \infty$ the solution is known to be bounded and not to include any incoming waves.

To complete the statement of the problem, initial conditions must be given in the entire domain $\Omega \cup D$ at time $t = 0$. In Ω the general initial conditions

$$u = u_0 \; , \quad \dot{u} = v_0 \qquad \text{in} \quad \Omega \quad \text{at} \quad t = 0 \tag{5}$$

are given. In D it is assumed that the medium is initially at rest, namely,

$$u = 0 \; , \quad \dot{u} = 0 \qquad \text{in} \quad D \quad \text{at} \quad t = 0 \; . \tag{6}$$

The goal is to solve the problem in the finite domain Ω via FEs. To this end, the artificial boundary $\mathcal{B}$ is now introduced at $x = x_{\mathcal{B}}$ to divide between Ω and D; see Fig. 1(b). It will be assumed that all the equations and conditions stated above which hold in D hold also on $\mathcal{B}$. To obtain a well-posed problem in Ω one must impose a boundary condition on $\mathcal{B}$. This has to be a NRBC so as to prevent spurious reflection of waves. The construction of this NRBC is discussed in the next section.

3. High-Order Non-Reflecting Boundary Conditions

3.1 The Higdon NRBC

The starting point for developing the high-order NRBCs on $\mathcal{B}$ is the sequence of NRBCs proposed by Higdon [43]. The Higdon NRBC of order J is

$$H_J: \qquad \left[\prod_{j=1}^{J}\left(\frac{\partial}{\partial t}+C_j\frac{\partial}{\partial x}\right)\right]u=0 \qquad \text{on} \quad \mathcal{B}\ . \tag{7}$$

Here, the C_j are constant parameters which have to be chosen and which signify phase speeds in the x-direction. Note that the first-order condition H_1 is a Sommerfeld-like boundary condition.

The Higdon conditions possess a few favorable properties. First, they are very *general*, namely they apply to a variety of wave problems, in one, two and three dimensions and in various configurations. Moreover, they can be used, without any difficulty, for wave problems in *dispersive* and *stratified* media. Most other available NRBCs are either designed for non-dispersive homogeneous media (as in acoustics and electromagnetics) or are inherently of low order (as in meteorology and oceanography).

Second, the boundary condition (7) is *exact* for all plane waves that propagate with an x-direction phase speed equal to either of $C_1, \ldots, C_J$. To see this, consider a wave which satisfies eq. (2) in D and the boundary condition (3) on Γ_S and Γ_N. Such a wave has the form

$$u=A\cos\left(\frac{n\pi y}{b}\right)\ \cos k(x-C_xt+\psi)\ , \qquad n=0,1,2,\ldots \tag{8}$$

where

$$C_x=\frac{\omega}{k}\ . \tag{9}$$

In (8) and (9), A is the wave amplitude, ψ is its phase, k is the x-component wave number, ω is the wave frequency and C_x is the x-direction phase velocity. It is common to refer to n as the "mode number." The wave number k, the frequency ω and the mode number n depend on each other through the dispersion relation. In D, where C_0 and f are constant, the dispersion relation is

$$\omega_n^2=C_0^2\left(k^2+\frac{n^2\pi^2}{b^2}\right)+f^2 \qquad , \qquad n=0,1,2,\ldots\ . \tag{10}$$

In general, solutions of (2) and (3) consist of an infinite number of plane waves of the form (8). There are also solutions that decay exponentially in the x direction; however, they are usually not of great concern, since the decaying modes are expected to be insignificant at the time they reach $\mathcal{B}$. Now, it is easy to verify that if one of the C_j's in (7) is equal to C_x, then the wave (8) satisfies the boundary condition (7) exactly.

Third, the Higdon NRBCs allow a relatively easy accuracy control. It can be shown (see Higdon [43] for a similar setting) that when a plane wave of the form (8) impinges on the boundary $\mathcal{B}$ where the NRBC H_J is imposed, the resulting *reflection coefficient* is

$$R = \prod_{j=1}^{J} \left| \frac{C_j - C_x}{C_j + C_x} \right| \ . \tag{11}$$

Again one sees that if $C_j = C_x$ for any one of the j's then $R = 0$, namely there is no reflection and the NRBC is exact. Moreover, one sees that the reflection coefficient is a product of J factors, *each of which is smaller than 1.* This implies that the reflection coefficient becomes smaller as the order J increases regardless of the choice made for the parameters C_j. Of course, a good choice for the C_j would lead to better accuracy with a lower order J, but even if one misses the correct C_j's considerably (say, with the simplest choice $C_j = C_0$ for $j = 1, \ldots, J$), one is still guaranteed to reduce the spurious reflection as the order J increases. This is an important property of Higdon's NRBCs and is the reason for their robustness.

Fourth, for certain choices of the parameters, the Higdon NRBCs are equivalent to NRBCs that are derived from rational approximation of the dispersion relation (the Engquist-Majda conditions [2] being the most well-known example). This has been proved by Higdon in [43]. Thus, the Higdon NRBCs can be viewed as *generalization* of rational-approximation NRBCs.

Despite all these advantages, the Higdon NRBCs have not been used extensively in the past. The reasons for this are as follows:

- For $J \geq 2$, the Higdon NRBCs are not compatible with the FE method. They have been used in the past only with finite difference discretization.

- Explicit finite difference formulas for the discrete Higdon conditions were developed in the literature up to third order only, because of their *algebraic complexity* which increases rapidly with the order. Thus, although in theory (7) is written as a high-order

NRBC, only the low-order Higdon conditions have been used in practice. Recently, Givoli and Neta constructed finite difference schemes based on high-order Higdon conditions [44, 45].

- The NRBC H_J involves *high normal and temporal derivatives*, up to order J. These pose obvious numerical difficulties.

- Until recently, no procedure has been provided in the literature for the *automatic* choice of the parameters C_j's which appear in the Higdon NRBCs. In [44] such a procedure has been devised and incorporated in a finite difference scheme.

Starting from the Higdon NRBCs (7), new NRBCs are now derived which are free from all these difficulties and are designed to fit the FE methodology.

3.2 The New High-Order NRBCs

The H_J condition (7) is first replaced by the equivalent condition

$$H_J : \qquad \left[\prod_{j=1}^{J}\left(\frac{\partial}{\partial x}+\frac{1}{C_j}\frac{\partial}{\partial t}\right)\right] u = 0 \quad \text{on} \quad \mathcal{B} \ . \tag{12}$$

Now the auxiliary functions $\phi_1, \ldots, \phi_{J-1}$ are introduced. These functions are defined on $\mathcal{B}$ as well as in the exterior domain D. Eventually they will be used only on $\mathcal{B}$, but the derivation requires that they be defined in D as well, or at least in a non-vanishing region adjacent to $\mathcal{B}$. The functions ϕ_j are defined via the relations

$$\left(\frac{\partial}{\partial x}+\frac{1}{C_1}\frac{\partial}{\partial t}\right) u = \phi_1 \ , \tag{13}$$

$$\left(\frac{\partial}{\partial x}+\frac{1}{C_2}\frac{\partial}{\partial t}\right) \phi_1 = \phi_2 \ , \tag{14}$$

$$\vdots$$

$$\left(\frac{\partial}{\partial x}+\frac{1}{C_J}\frac{\partial}{\partial t}\right) \phi_{J-1} = 0 \ . \tag{15}$$

By definition, these relations hold in D, and also on $\mathcal{B}$. It is easy to see that (13)–(15), when imposed as boundary conditions on $\mathcal{B}$, are equivalent to the single boundary condition (12).

By defining

$$\phi_0 \equiv u \qquad , \qquad \phi_J \equiv 0 \ , \tag{16}$$

eqs. (13)–(15) can be written concisely as

$$\left(\frac{\partial}{\partial x} + \frac{1}{C_j}\frac{\partial}{\partial t}\right)\phi_{j-1} = \phi_j \qquad , \qquad j = 1, \ldots, J \ . \tag{17}$$

This set of conditions involves only first-order derivatives. However, due to the appearance of the x-derivative in (17), the ϕ_j cannot be discretized on the boundary $\mathcal{B}$ alone. Therefore (17) will be manipulated in order to get rid of the x-derivative.

The function u satisfies the wave equation (2) in D. The function ϕ_1 is obtained by applying the linear operator $\partial/\partial x + (1/C_1)\partial/\partial t$ to u, as in (13); hence it is clear that ϕ_1 also satisfies the same equation in D. Similarly, it can be deduced that each of the functions ϕ_j satisfies a wave equation like (2), namely,

$$\ddot{\phi}_j - C_0^2 \ \nabla^2\phi_j + f^2 \ \phi_j = 0 \qquad \text{in} \quad D \ . \tag{18}$$

Another way of writing this equation is

$$\frac{\partial^2\phi_j}{\partial x^2} + \frac{\partial^2\phi_j}{\partial y^2} - \frac{1}{C_0^2}\ddot{\phi}_j - \frac{f^2}{C_0^2}\phi_j = 0 \ . \tag{19}$$

Now, the following identity is used:

$$\frac{\partial^2\phi_j}{\partial x^2} = \left(\frac{\partial}{\partial x} - \frac{1}{C_{j+1}}\frac{\partial}{\partial t}\right)\left(\frac{\partial}{\partial x} + \frac{1}{C_{j+1}}\frac{\partial}{\partial t}\right)\phi_j + \frac{1}{C_{j+1}^2}\ddot{\phi}_j \ . \tag{20}$$

Substituting (20) in (19) and replacing j with $j-1$ everywhere yields, for $j = 1, \ldots, J$,

$$\left(\frac{\partial}{\partial x} - \frac{1}{C_j}\frac{\partial}{\partial t}\right)\left(\frac{\partial}{\partial x} + \frac{1}{C_j}\frac{\partial}{\partial t}\right)\phi_{j-1} + \left(\frac{1}{C_j^2} - \frac{1}{C_0^2}\right)\ddot{\phi}_{j-1} + \frac{\partial^2\phi_{j-1}}{\partial y^2} - \frac{f^2}{C_0^2}\phi_{j-1} = 0 \ . \tag{21}$$

From this and (17) one gets, for $j = 1, \ldots, J$,

$$\left(\frac{\partial}{\partial x} - \frac{1}{C_j}\frac{\partial}{\partial t}\right)\phi_j + \left(\frac{1}{C_j^2} - \frac{1}{C_0^2}\right)\ddot{\phi}_{j-1} + \frac{\partial^2\phi_{j-1}}{\partial y^2} - \frac{f^2}{C_0^2}\phi_{j-1} = 0 \ . \tag{22}$$

On the other hand, (17) can also be written as

$$\left(\frac{\partial}{\partial x} + \frac{1}{C_{j+1}}\frac{\partial}{\partial t}\right)\phi_j = \phi_{j+1} \ , \qquad j = 0, \ldots, J-1 \ . \tag{23}$$

Subtracting (22) from (23) finally gives, for $j = 1, \ldots, J-1$,

$$\left(\frac{1}{C_j} + \frac{1}{C_{j+1}}\right)\dot{\phi}_j = \phi_{j+1} + \left(\frac{1}{C_j^2} - \frac{1}{C_0^2}\right)\ddot{\phi}_{j-1} + \frac{\partial^2 \phi_{j-1}}{\partial y^2} - \frac{f^2}{C_0^2}\phi_{j-1} \ . \tag{24}$$

As desired, the new boundary condition (24) does not involve x-derivatives. In addition, there are no high y- and t-derivatives in (24) beyond second order.

Rewriting (13), (24) and (16), the new formulation of the Jth-order NRBC on $\mathcal{B}$ can be summarized as follows:

$$\beta_0 \dot{u} + \frac{\partial u}{\partial x} = \phi_1 \ , \tag{25}$$

$$\beta_j \dot{\phi}_j - \alpha_j \ddot{\phi}_{j-1} - \phi''_{j-1} + \lambda \phi_{j-1} = \phi_{j+1} \qquad , \qquad j = 1, \ldots, J-1 \ , \tag{26}$$

$$\alpha_j = \frac{1}{C_j^2} - \frac{1}{C_0^2} \quad , \quad \beta_0 = \frac{1}{C_1} \quad , \quad \beta_j = \frac{1}{C_j} + \frac{1}{C_{j+1}} \quad , \quad \lambda = \frac{f^2}{C_0^2} \ , \tag{27}$$

$$\phi_0 \equiv u \qquad , \qquad \phi_J \equiv 0 \ . \tag{28}$$

In (26) and elsewhere, a prime indicates differentiation with respect to y along $\mathcal{B}$, i.e., the tangential derivative on $\mathcal{B}$.

It will be beneficial to also write the NRBC (25)–(28) in a matrix form. To this end the J-dimensional vector of unknowns

$$\boldsymbol{U}^T = \left\{ \begin{array}{ccccc} u & \phi_1 & \phi_2 & \ldots & \phi_{J-1} \end{array} \right\} \tag{29}$$

is defined on $\mathcal{B}$. Here the ^{T} denotes transposition. With this definition, (25)–(28) can be written in the form

$$-\frac{\partial u}{\partial x}\boldsymbol{e}_1 = \boldsymbol{A}\boldsymbol{U} + \boldsymbol{B}\dot{\boldsymbol{U}} + \boldsymbol{D}\ddot{\boldsymbol{U}} - \boldsymbol{E}\boldsymbol{U}'' \qquad \text{on} \quad \mathcal{B} \ . \tag{30}$$

Here $\boldsymbol{e}_1$ is the J-dimensional vector defined by

$$\boldsymbol{e}_1^T = \left\{ \begin{array}{ccccc} 1 & 0 & 0 & \ldots & 0 \end{array} \right\} \ . \tag{31}$$

The four J-dimensional matrices appearing in (30) are:

$$\boldsymbol{A} = \begin{bmatrix} 0 & -1 & 0 & 0 & \ldots & 0 \\ \lambda & 0 & -1 & 0 & \ldots & 0 \\ 0 & \lambda & 0 & -1 & \ldots & 0 \\ \vdots & \vdots & \ddots & \ddots & \ddots & \vdots \\ 0 & \ldots & 0 & \lambda & 0 & -1 \\ 0 & \ldots & 0 & 0 & \lambda & 0 \end{bmatrix} \ , \qquad \boldsymbol{B} = \begin{bmatrix} \beta_0 & 0 & 0 & 0 & \ldots & 0 \\ 0 & \beta_1 & 0 & 0 & \ldots & 0 \\ 0 & 0 & \beta_2 & 0 & \ldots & 0 \\ \vdots & \vdots & \ddots & \ddots & \ddots & \vdots \\ 0 & \ldots & 0 & 0 & \beta_{J-2} & 0 \\ 0 & \ldots & 0 & 0 & 0 & \beta_{J-1} \end{bmatrix} \tag{32}$$

$$\boldsymbol{D} = \begin{bmatrix} 0 & 0 & 0 & 0 & \dots & 0 \\ -\alpha_1 & 0 & 0 & 0 & \dots & 0 \\ 0 & -\alpha_2 & 0 & 0 & \dots & 0 \\ \vdots & \vdots & \ddots & \ddots & \ddots & \vdots \\ 0 & \dots & 0 & -\alpha_{J-2} & 0 & 0 \\ 0 & \dots & 0 & 0 & -\alpha_{J-1} & 0 \end{bmatrix}, \qquad \boldsymbol{E} = \begin{bmatrix} 0 & 0 & 0 & 0 & \dots & 0 \\ 1 & 0 & 0 & 0 & \dots & 0 \\ 0 & 1 & 0 & 0 & \dots & 0 \\ \vdots & \vdots & \ddots & \ddots & \ddots & \vdots \\ 0 & \dots & 0 & 1 & 0 & 0 \\ 0 & \dots & 0 & 0 & 1 & 0 \end{bmatrix} \tag{33}$$

Note the tridiagonal structure of these four matrices. Note also that the matrices $\boldsymbol{A}$, $\boldsymbol{D}$ and $\boldsymbol{E}$ are non-symmetric.

4. Finite Element Semi-Discrete Formulation

The problem to be solved in Ω consists of the inhomogeneous wave equation (1), the initial conditions (5), the north and south boundary condition (3), the west boundary condition (4), and the east NRBC given by (25)–(28) or equivalently by (30).

Two FE formulations will be presented here: an augmented one and a split one.

4.1 The Augmented FE Formulation

First, the weak (or variational) form of the problem in Ω is constructed. The solution u is sought in the space of trial functions,

$$\mathcal{S} = \{\ u \mid u \in H^1(\Omega) \qquad \& \qquad u = u_W \quad \text{on} \quad \Gamma_W\ \}\ . \tag{34}$$

Here $H^1(\Omega)$ is the Sobolev space of square-integrable functions in Ω. Now, eq. (1) is multiplied by the arbitrary weight function $w \in \mathcal{S}_0$, where

$$\mathcal{S}_0 = \{\ w \mid w \in H^1(\Omega) \qquad \& \qquad w = 0 \quad \text{on} \quad \Gamma_W\ \}\ , \tag{35}$$

and the result is integrated over Ω. This yields, after integration by parts,

$$\int_\Omega w\ddot{u}\, d\Omega + \int_\Omega (\boldsymbol{\nabla} w \cdot C_0^2 \boldsymbol{\nabla} u + w f^2 u)\, d\Omega - \int_B w C_0^2 \frac{\partial u}{\partial x}\, d\mathcal{B} = \int_\Omega wS\, d\Omega\ , \tag{36}$$

for $u \in \mathcal{S}$ and for all $w \in \mathcal{S}_0$. The integral over $\mathcal{B}$ on the left side of (36) will involve the auxiliary functions ϕ_j. In analogy to (29), a vector of weight functions is defined, i.e.,

$$\boldsymbol{W}^T = \left\{ \begin{array}{ccccc} w & \tau_1 & \tau_2 & \ldots & \tau_{J-1} \end{array} \right\} , \tag{37}$$

where the τ_j are arbitrary weight functions associated with the ϕ_j. In (29) and (37), u and w are defined in Ω, whereas the ϕ_j and τ_j are defined on $\mathcal{B}$. With these definitions, the integral over $\mathcal{B}$ in (36) is calculated by using the NRBC (30):

$$\begin{aligned} -\int_B w\frac{\partial u}{\partial x}\, d\mathcal{B} &= -\int_B \boldsymbol{W}\cdot\boldsymbol{e}_1\, \frac{\partial u}{\partial x}\, d\mathcal{B} = \int_B \boldsymbol{W}\, \left(\boldsymbol{A}\boldsymbol{U} + \boldsymbol{B}\dot{\boldsymbol{U}} + \boldsymbol{D}\ddot{\boldsymbol{U}} - \boldsymbol{E}\boldsymbol{U}''\right) d\mathcal{B} \\ &= \int_B \boldsymbol{W}\boldsymbol{A}\boldsymbol{U}\, d\mathcal{B} + \int_B \boldsymbol{W}\boldsymbol{B}\dot{\boldsymbol{U}}\, d\mathcal{B} + \int_B \boldsymbol{W}\boldsymbol{D}\ddot{\boldsymbol{U}}\, d\mathcal{B} + \int_B \boldsymbol{W}'\boldsymbol{E}\boldsymbol{U}'\, d\mathcal{B} \ . \end{aligned} \tag{38}$$

The last equality in (38) is obtained by integration by parts, where the contribution from the boundary of $\mathcal{B}$ vanishes due to (3). Using (38) in (36), the weak form of the problem in Ω follows:

Find $\boldsymbol{U} \in \hat{\mathcal{S}}$ *such that for all* $\boldsymbol{W} \in \hat{\mathcal{S}}_0$,

$$d(\boldsymbol{W}\,,\,\ddot{\boldsymbol{U}}) + a(\boldsymbol{W}\,,\,\boldsymbol{U}) + b_0(\boldsymbol{W}\,,\,\boldsymbol{U}) + b_1(\boldsymbol{W}\,,\,\dot{\boldsymbol{U}}) + b_2(\boldsymbol{W}\,,\,\ddot{\boldsymbol{U}}) = L(\boldsymbol{W}) \ , \tag{39}$$

where

$$\hat{\mathcal{S}} = \{\ \boldsymbol{U} \mid U_1 \in \mathcal{S}\ , \qquad U_j \in H^1(\mathcal{B}) \quad \text{for} \quad j = 2, \ldots, J\ \}\ , \tag{40}$$

$$\hat{\mathcal{S}}_0 = \{\ \boldsymbol{W} \mid W_1 \in \mathcal{S}_0\ , \qquad W_j \in H^1(\mathcal{B}) \quad \text{for} \quad j = 2, \ldots, J\ \}\ , \tag{41}$$

$$d(\boldsymbol{W}\,,\,\ddot{\boldsymbol{U}}) = \int_\Omega W_1\ddot{U}_1\, d\Omega\ , \tag{42}$$

$$a(\boldsymbol{W}\,,\,\boldsymbol{U}) = \int_\Omega \left(\boldsymbol{\nabla}W_1\cdot C_0^2\boldsymbol{\nabla}U_1 + W_1 f^2 U_1\right) d\Omega\ , \tag{43}$$

$$b_0(\boldsymbol{W}\,,\,\boldsymbol{U}) = \int_B C_0^2\left(\boldsymbol{W}\boldsymbol{A}\boldsymbol{U} + \boldsymbol{W}'\boldsymbol{E}\boldsymbol{U}'\right) d\mathcal{B}\ , \tag{44}$$

$$b_1(\boldsymbol{W}\,,\,\dot{\boldsymbol{U}}) = \int_B C_0^2\boldsymbol{W}\boldsymbol{B}\dot{\boldsymbol{U}}\, d\mathcal{B}\ , \tag{45}$$

$$b_2(\boldsymbol{W}\,,\,\ddot{\boldsymbol{U}}) = \int_B C_0^2\boldsymbol{W}\boldsymbol{D}\ddot{\boldsymbol{U}}\, d\mathcal{B}\ , \tag{46}$$

$$L(\boldsymbol{W}) = \int_\Omega W_1 S\, d\Omega\ . \tag{47}$$

The Galerkin FE method is used to discretize this problem in space. In each element, the functions $\boldsymbol{W}(\boldsymbol{x}) = \{W_j(\boldsymbol{x})\}$ and $\boldsymbol{U}(\boldsymbol{x},t) = \{U_j(\boldsymbol{x},t)\}$ are replaced by their finite-dimensional

approximations

$$W_j^e(\boldsymbol{x}) = \sum_{a=1}^{N_{en}} \bar{W}_{ja}^e N_a^{(j)}(\boldsymbol{x}) \qquad , \qquad U_j^e(\boldsymbol{x},t) = \sum_{a=1}^{N_{en}} \bar{U}_{ja}^e(t) N_a^{(j)}(\boldsymbol{x}) \, , \qquad \boldsymbol{x} \equiv (x,y) \in \Omega^e \, . \tag{48}$$

Here Ω^e is the domain of element e, $N_a^{(j)}(\boldsymbol{x})$ is the element shape function associated with variable U_j and node a, N_{en} is the number of element nodes, and $\bar{U}_{ja}^e(t)$ is the unknown value of the variable U_j at node a of element e and time t. (No summation is implied in this paper for repeated indices.) Similar expressions can be written on the global level too. Note that in (48) different shape functions, $N_a^{(j)}$, are assigned to the different variables U_j. It is convenient to take the same shape functions for all the variables, namely $N_a^{(j)} \equiv N_a$, but one has to address the issue of numerical stability. See discussion in Section 6. Using the approximations (48) in the weak form of the problem (39) leads to the following linear system of ordinary differential equations (ODEs) in time:

$$\bar{\boldsymbol{M}} \ddot{\bar{\boldsymbol{U}}}(t) + \bar{\boldsymbol{C}} \dot{\bar{\boldsymbol{U}}}(t) + \bar{\boldsymbol{K}} \bar{\boldsymbol{U}}(t) = \bar{\boldsymbol{S}}(t) \, . \tag{49}$$

Here $\bar{\boldsymbol{M}}$ is the mass matrix, $\bar{\boldsymbol{C}}$ is the damping matrix, $\bar{\boldsymbol{K}}$ is the stiffness matrix, $\bar{\boldsymbol{S}}$ is the load vector, and $\bar{\boldsymbol{U}}(t)$ is the vector of unknowns, whose entries are the unknown nodal values of the variables u and ϕ_j, for $j = 1, \ldots, J-1$. All these are global-level arrays, with dimension $N + (J-1)N_{\mathcal{B}}$, where N is the total number of 'u' degrees of freedom and $N_{\mathcal{B}}$ is the number of nodes on $\mathcal{B}$. The system (49) is accompanied by appropriate initial conditions. The vector of initial values is easily obtained: it depends solely on the given functions u_0 and v_0 (see (5)) since all the auxiliary variables ϕ_j are defined along $\mathcal{B}$ only, and thus vanish identically at time $t = 0$.

As usual in the FE method, the global arrays $\bar{\boldsymbol{M}}$, $\bar{\boldsymbol{C}}$, $\bar{\boldsymbol{K}}$ and $\bar{\boldsymbol{S}}$ appearing in (49) are formed by calculating and assembling together the analogous arrays on the element level, $\bar{\boldsymbol{m}}^e$, $\bar{\boldsymbol{c}}^e$, $\bar{\boldsymbol{k}}^e$ and $\bar{\boldsymbol{s}}^e$. Thus,

$$\bar{\boldsymbol{M}} = \mathop{\mathcal{A}}_{e=1}^{N_{el}} \bar{\boldsymbol{m}}^e \qquad , \qquad \bar{\boldsymbol{C}} = \mathop{\mathcal{A}}_{e=1}^{N_{el}} \bar{\boldsymbol{c}}^e \qquad , \qquad \bar{\boldsymbol{K}} = \mathop{\mathcal{A}}_{e=1}^{N_{el}} \bar{\boldsymbol{k}}^e \qquad , \qquad \bar{\boldsymbol{S}} = \mathop{\mathcal{A}}_{e=1}^{N_{el}} \bar{\boldsymbol{s}}^e \, , \tag{50}$$

where $\mathop{\mathcal{A}}_{e=1}^{N_{el}}$ is the assembly operator and N_{el} is the total number of elements. The expressions for the element matrices and vector are:

$$\bar{\boldsymbol{m}}^e = \bar{\boldsymbol{m}}^{\Omega e} + \bar{\boldsymbol{m}}^{\mathcal{B}e} \, , \qquad \bar{\boldsymbol{k}}^e = \bar{\boldsymbol{k}}^{\Omega e} + \bar{\boldsymbol{k}}^{\mathcal{B}e} \, , \tag{51}$$

$$\bar{\boldsymbol{m}}^{\Omega e} = \left[\bar{m}^{\Omega e}_{(ai)(bj)}\right] \ , \qquad \bar{\boldsymbol{m}}^{\mathcal{B}e} = \left[\bar{m}^{\mathcal{B}e}_{(ai)(bj)}\right] \ , \qquad \bar{\boldsymbol{c}}^{e} = \left[\bar{c}^{e}_{(ai)(bj)}\right] \ , \tag{52}$$

$$\bar{\boldsymbol{k}}^{\Omega e} = \left[\bar{k}^{\Omega e}_{(ai)(bj)}\right] \ , \qquad \bar{\boldsymbol{k}}^{\mathcal{B}e} = \left[\bar{k}^{\mathcal{B}e}_{(ai)(bj)}\right] \ , \qquad \bar{\boldsymbol{s}}^{e} = \left\{\bar{s}^{e}_{(ai)}\right\} \ , \tag{53}$$

$$\bar{m}^{\Omega e}_{(ai)(bj)} = \delta_{i1}\delta_{j1}\int_{\Omega^e} N_a^{(i)} N_b^{(j)}\, d\Omega \ , \tag{54}$$

$$\bar{k}^{\Omega e}_{(ai)(bj)} = \delta_{i1}\delta_{j1}\int_{\Omega^e} (\boldsymbol{\nabla} N_a^{(i)} \cdot C_0^2 \boldsymbol{\nabla} N_b^{(j)} + N_a^{(i)} f^2 N_b^{(j)})\, d\Omega \ , \tag{55}$$

$$\bar{m}^{\mathcal{B}e}_{(ai)(bj)} = \int_{B^e} N_a^{(i)} C_0^2 D_{ij} N_b^{(j)}\, d\mathcal{B} \ , \tag{56}$$

$$\bar{c}^{e}_{(ai)(bj)} = \int_{B^e} N_a^{(i)} C_0^2 B_{ij} N_b^{(j)}\, d\mathcal{B} \ , \tag{57}$$

$$\bar{k}^{\mathcal{B}e}_{(ai)(bj)} = \int_{B^e} C_0^2 \left(N_a^{(i)} A_{ij} N_b^{(j)} + N_a^{(i)'} E_{ij} N_b^{(j)'}\right) d\mathcal{B} \ , \tag{58}$$

$$\bar{s}^{e}_{(ai)} = \delta_{i1}\int_{\Omega^e} N_a^{(i)} S\, d\Omega - \delta_{i1}\sum_{b=1}^{N_{en}} \bar{k}^{\Omega e}_{(a1)(b1)} (u_W)^e_b \ . \tag{59}$$

Here (ai) is the index associated with node a and "degree of freedom" i (for $i = 1, \ldots, J$), and similarly for (bj). Also, δ_{ij} is the Kronecker delta, Ω^e and $\mathcal{B}^e$ denote, respectively, the part of Ω and $\mathcal{B}$ associated with element e, and $(u_W)^e_b$ is defined to be the value of the given west-boundary function u_W at node b of element e if this node is on Γ_W, and zero otherwise.

The FE formulation (49)–(59) is a mixed C^0 formulation. The matrices $\bar{\boldsymbol{m}}^{\Omega e}$ and $\bar{\boldsymbol{k}}^{\Omega e}$ and the vector $\bar{\boldsymbol{s}}^{e}$ are the standard element mass and stiffness matrices and load vector. More precisely, each of them consists of a nonzero-block which is standard, and corresponds to $i = j = 1$, namely to the 'u' degree of freedom, and additional zero rows and columns corresponding to the auxiliary degrees of freedom. The element matrices $\bar{\boldsymbol{m}}^{\mathcal{B}e}$, $\bar{\boldsymbol{c}}^{e}$ and $\bar{\boldsymbol{k}}^{\mathcal{B}e}$ are contributed by the NRBC on $\mathcal{B}$. They are nonzero only for elements with nonempty $\mathcal{B}^e$, namely for elements that have a boundary on $\mathcal{B}$. Note that the *damping* term $\bar{\boldsymbol{C}}\dot{\bar{\boldsymbol{U}}}$ in (49) originates only from the NRBC on $\mathcal{B}$, the original problem involving no physical damping. All the element matrices except $\bar{\boldsymbol{m}}^{\mathcal{B}e}$ and $\bar{\boldsymbol{k}}^{\mathcal{B}e}$ are symmetric. The latter two, given by (56) and (58) are non-symmetric due to the asymmetry of the matrices $\boldsymbol{A}$, $\boldsymbol{D}$ and $\boldsymbol{E}$ in (32) and (33). The consequence of this is that the global mass and stiffness matrices $\bar{\boldsymbol{M}}$ and $\bar{\boldsymbol{K}}$ are also non-symmetric.

The dynamic system (49) may be solved by a standard time-integration method, such as one of the Newmark family of schemes [46].

4.2 The Split FE Formulation

The augmented FE formulation discussed in the previous subsection has two disadvantages: (a) it is non-symmetric, and (b) it involves large sparse global matrices whose entries are associated with both 'primary' and 'auxiliary' degrees of freedom. Now an alternative FE formulation is proposed, in which the global system of coupled equations is split to separate equations for the different variables. This formulation is symmetric and involves more compact matrices.

In the split formulation, the weak equation (36) is considered again, but now (25) is substituted directly into it, which yields:

$$\int_\Omega w\ddot{u}\,d\Omega + \int_\Omega (\boldsymbol{\nabla} w \cdot C_0^2 \boldsymbol{\nabla} u + w f^2 u)\,d\Omega + \int_B w C_0^2 \beta_0 \dot{u}\,d\mathcal{B} - \int_B w C_0^2 \phi_1\,d\mathcal{B} = \int_\Omega wS\,d\Omega\ , \quad (60)$$

for $u \in \mathcal{S}$ and for all $w \in \mathcal{S}_0$. This is not a complete weak form of the problem in Ω, since the unknown function ϕ_1 appears in the last term on the left side. Now a separate weak form can be obtained for eq. (26), by multiplying it by the weight function τ_j and integrating over $\mathcal{B}$. This yields, after integrating by parts (and using (3) to deduce that the boundary term vanishes),

$$\int_B \tau_j \beta_j \dot{\phi}_j\,d\mathcal{B} - \int_B \tau_j \alpha_j \ddot{\phi}_{j-1}\,d\mathcal{B} + \int_B \tau_j' \phi_{j-1}'\,d\mathcal{B} + \int_B \tau_j \lambda \phi_{j-1}\,d\mathcal{B} = \int_B \tau_j \phi_{j+1}\,d\mathcal{B}\ , \quad (61)$$

for $j = 1, \ldots, J-1$, for $\phi_j \in H^1(\mathcal{B})$ and any $\tau_j \in H^1(\mathcal{B})$. Recall that $\phi_0 \equiv u$ and $\phi_J \equiv 0$; see (28). Eqs. (60) and (61) together constitute a weak form of the problem, equivalent to (39), namely:

Find $u \in \mathcal{S}$ and $\phi_j \in H^1$, $j = 1, \ldots, J-1$, such that eqs. (60) and (61) are satisfied for all $w \in \mathcal{S}_0$ and $\tau_j \in H^1$.

This problem is now discretized in space using the Galerkin FE method. In each element, the functions $w(\boldsymbol{x})$, $u(\boldsymbol{x}, t)$, $\tau_j(\boldsymbol{x})$ and $\phi_j(\boldsymbol{x}, t)$ are replaced by their finite-dimensional approximations

$$w^e(\boldsymbol{x}) = \sum_{a=1}^{N_{en}} w_a^e N_a(\boldsymbol{x})\ , \qquad u^e(\boldsymbol{x}) = \sum_{a=1}^{N_{en}} d_a^e(t) N_a(\boldsymbol{x})\ , \qquad \boldsymbol{x} \equiv (x, y) \in \Omega^e\ , \quad (62)$$

$$\tau_j^e(\boldsymbol{x}) = \sum_{a=1}^{N_{en}} \tau_{ja}^e N_a^{(j)}(\boldsymbol{x})\ , \qquad \phi_j^e(\boldsymbol{x}) = \sum_{a=1}^{N_{en}} \phi_{ja}^e N_a^{(j)}(\boldsymbol{x})\ , \qquad \boldsymbol{x} \equiv (x, y) \in \mathcal{B}^e\ . \quad (63)$$

The notation used here is similar to that used in Subsection 4.1. As in the augmented formulation, different shape functions are assigned to the different variables: N_a for the variable u and $N_a^{(j)}$ for the variable ϕ_j. Again, it is convenient to take the same shape functions for all the variables; see discussion in Section 6.

These approximations are used in the weak equations (60) and (61). This leads to the following set of ODEs in time:

$$\boldsymbol{M}\ddot{\boldsymbol{d}} + \boldsymbol{C}\dot{\boldsymbol{d}} + \boldsymbol{K}\boldsymbol{d} = \boldsymbol{S} + \boldsymbol{G}\boldsymbol{\phi}_1 \ , \tag{64}$$

$$\boldsymbol{C}_j\dot{\boldsymbol{\phi}}_j = \boldsymbol{P}_j\ddot{\boldsymbol{\phi}}_{j-1} - \boldsymbol{Q}_j\boldsymbol{\phi}_{j-1} + \boldsymbol{R}_j\boldsymbol{\phi}_{j+1} \qquad , \qquad j = 1, \ldots, J-1 \ . \tag{65}$$

Here, $\boldsymbol{\phi}_j$ is the unknown vector whose entries are the nodal values of the variable ϕ_j on $\mathcal{B}$. In (64), $\boldsymbol{M}$, $\boldsymbol{C}$ and $\boldsymbol{K}$ are the standard $N \times N$ mass matrix, damping matrix and stiffness matrix, respectively, where N is the total number of 'u' degrees of freedom. Also, $\boldsymbol{S}$ is the load vector, $\boldsymbol{d}$ is the global unknown vector whose entries are the nodal values of u, and $\boldsymbol{G}$ is an $N \times N_{\mathcal{B}}$ rectangular matrix, where $N_{\mathcal{B}}$ is the number of nodes on $\mathcal{B}$. In (65), all the matrices are $N_{\mathcal{B}} \times N_{\mathcal{B}}$. Relating to (28), we have that $\boldsymbol{\phi}_J \equiv 0$, and that $\boldsymbol{\phi}_0$ is the $N_{\mathcal{B}}$-dimensional vector whose entries are equal to the entries of the N-dimensional vector $\boldsymbol{d}$ for the degrees of freedom on $\mathcal{B}$.

As before, all the global arrays are obtained from analogous element arrays via assembly, namely

$$\boldsymbol{M} = \mathop{\mathcal{A}}_{e=1}^{N_{el}} \boldsymbol{m}^e \qquad , \qquad \boldsymbol{C} = \mathop{\mathcal{A}}_{e=1}^{N_{el}} \boldsymbol{c}^e \qquad , \qquad \boldsymbol{K} = \mathop{\mathcal{A}}_{e=1}^{N_{el}} \boldsymbol{k}^e \ , \tag{66}$$

$$\boldsymbol{S} = \mathop{\mathcal{A}}_{e=1}^{N_{el}} \boldsymbol{s}^e \qquad , \qquad \boldsymbol{G} = \mathop{\mathcal{A}}_{e=1}^{N_{el}} \boldsymbol{g}^e \qquad , \qquad \boldsymbol{C}_j = \mathop{\mathcal{A}}_{e=1}^{N_{el}} \boldsymbol{c}_j^e \ , \tag{67}$$

$$\boldsymbol{P}_j = \mathop{\mathcal{A}}_{e=1}^{N_{el}} \boldsymbol{p}_j^e \qquad , \qquad \boldsymbol{Q}_j = \mathop{\mathcal{A}}_{e=1}^{N_{el}} \boldsymbol{q}_j^e \qquad , \qquad \boldsymbol{R}_j = \mathop{\mathcal{A}}_{e=1}^{N_{el}} \boldsymbol{r}_j^e \ . \tag{68}$$

The expressions for the element arrays are:

$$\boldsymbol{m}^e = [m_{ab}^e] \qquad , \qquad \boldsymbol{c}^e = [c_{ab}^e] \qquad , \qquad \boldsymbol{k}^e = [k_{ab}^e] \ , \tag{69}$$

$$\boldsymbol{s}^e = \{s_a^e\} \qquad , \qquad \boldsymbol{g}^e = [g_{ab}^e] \qquad , \qquad \boldsymbol{c}_j^e = \left[(c_j^e)_{ab}\right] \ , \tag{70}$$

$$\boldsymbol{p}_j^e = \left[(p_j^e)_{ab}\right] \qquad , \qquad \boldsymbol{q}_j^e = \left[(q_j^e)_{ab}\right] \qquad , \qquad \boldsymbol{r}_j^e = \left[(r_j^e)_{ab}\right] \ , \tag{71}$$

$$m_{ab}^e = \int_{\Omega^e} N_a N_b \, d\Omega \ , \tag{72}$$

$$k^e_{ab} = \int_{\Omega^e} \left(\boldsymbol{\nabla} N_a \cdot C_0^2 \boldsymbol{\nabla} N_b + N_a f^2 N_b \right) d\Omega \ , \tag{73}$$

$$s^e_a = \int_{\Omega^e} N_a S \, d\Omega - \sum_{b=1}^{N_{en}} k^e_{ab} (u_W)^e_b \ , \tag{74}$$

$$c^e_{ab} = \int_{\mathcal{B}^e} \beta_0 C_0^2 N_a N_b \, d\mathcal{B} \ , \tag{75}$$

$$g^e_{ab} = \int_{\mathcal{B}^e} C_0^2 N_a N_b^{(1)} \, d\mathcal{B} \ , \tag{76}$$

$$(c^e_j)_{ab} = \int_{\mathcal{B}^e} \beta_j N_a^{(j)} N_b^{(j)} \, d\mathcal{B} \ , \tag{77}$$

$$(p^e_j)_{ab} = \int_{\mathcal{B}^e} \alpha_j N_a^{(j)} N_b^{(j-1)} \, d\mathcal{B} \ , \tag{78}$$

$$(q^e_j)_{ab} = \int_{\mathcal{B}^e} \left(N_a^{(j)\prime} N_b^{(j-1)\prime} + \lambda N_a^{(j)} N_b^{(j-1)} \right) d\mathcal{B} \ , \tag{79}$$

$$(r^e_j)_{ab} = \int_{\mathcal{B}^e} N_a^{(j)} N_b^{(j+1)} \, d\mathcal{B} \ . \tag{80}$$

It is clear that the element matrices $\boldsymbol{m}^e$, $\boldsymbol{c}^e$, $\boldsymbol{k}^e$ and $\boldsymbol{c}^e_j$, and hence also the global matrices $\boldsymbol{M}$, $\boldsymbol{C}$, $\boldsymbol{K}$ and $\boldsymbol{C}_j$, are *symmetric*. These global matrices are the ones which appear on the left sides of the ODEs (64) and (65), and whose symmetry is beneficial for the time-integration scheme discussed in the next section. The symmetry of the other global square matrices $\boldsymbol{P}_j$, $\boldsymbol{Q}_j$ and $\boldsymbol{R}_j$ is less important since they appear on the right hand sides of (64) and (65), as "loading terms." Nevertheless, if all the shape functions $N_a^{(j)}$ are the same (i.e., independent of j), then the element matrices $\boldsymbol{p}^e_j$, $\boldsymbol{q}^e_j$ and $\boldsymbol{r}^e_j$, and hence $\boldsymbol{P}_j$, $\boldsymbol{Q}_j$ and $\boldsymbol{R}_j$, are symmetric too.

5. Solution of the Dynamic System

A time-integration scheme is proposed now for the solution of (64) and (65), which constitute J coupled systems of ODEs. Each of these systems is discretized based on the Newmark family of schemes for second-order ODEs in time [46]. This family has two parameters, $0 \leq \beta \leq 1/2$ and $0 \leq \gamma \leq 1$, which control the accuracy and stability of the scheme. Note that the system (65) is actually first-order in time for $\boldsymbol{\phi}_j$, so that the "mass matrix" is zero for this system. However, one can still use the Newmark method as long as the "damping matrix" $\boldsymbol{C}_j$ is non-singular, which is indeed the case. The advantage of using the Newmark scheme for (65) (as opposed, say, to using the generalized trapezoidal scheme [46]) is that

it yields the "acceleration," namely $\boldsymbol{\phi}_j$, in each time-step. This "acceleration" is needed because it appears in the right side of (65).

The approximations of $\boldsymbol{d}$, $\dot{\boldsymbol{d}}$ and $\ddot{\boldsymbol{d}}$ at time-step n are denoted by $\boldsymbol{d}_n$, $\boldsymbol{v}_n$ and $\boldsymbol{a}_n$, respectively. Also, the approximations of $\boldsymbol{\phi}_j$ and $\dot{\boldsymbol{\phi}}_j$ and $\ddot{\boldsymbol{\phi}}_j$ at time-step n are denoted by $\boldsymbol{\phi}_{j,n}$, $\boldsymbol{V}_{j,n}$ and $\boldsymbol{A}_{j,n}$, respectively.

In predictor-corrector form, the proposed time-integration scheme is:

Prediction:

$$\tilde{\boldsymbol{d}}_{n+1} = \boldsymbol{d}_n + \Delta t \boldsymbol{v}_n + \frac{\Delta t^2}{2}(1-2\beta)\boldsymbol{a}_n \tag{81}$$

$$\tilde{\boldsymbol{v}}_{n+1} = \boldsymbol{v}_n + (1-\gamma)\Delta t \boldsymbol{a}_n \tag{82}$$

$$\tilde{\boldsymbol{\phi}}_{j,n+1} = \boldsymbol{\phi}_{j,n} + \Delta t \boldsymbol{V}_{j,n} + \frac{\Delta t^2}{2}(1-2\beta)\boldsymbol{A}_{j,n} \quad , \quad j = 1, \ldots, J-1 \tag{83}$$

$$\tilde{\boldsymbol{V}}_{j,n+1} = \boldsymbol{V}_{j,n} + (1-\gamma)\Delta t \boldsymbol{A}_{j,n} \quad , \quad j = 1, \ldots, J-1 \tag{84}$$

Solution:

$$(\boldsymbol{M} + \gamma\Delta t \boldsymbol{C} + \beta \Delta t^2 \boldsymbol{K})\boldsymbol{a}_{n+1} = \boldsymbol{S}_{n+1} + \boldsymbol{G}\tilde{\boldsymbol{\phi}}_{1,n+1} - \boldsymbol{C}\tilde{\boldsymbol{v}}_{n+1} - \boldsymbol{K}\tilde{\boldsymbol{d}}_{n+1} \tag{85}$$

$$\gamma\Delta t \boldsymbol{C}_j \boldsymbol{A}_{j,n+1} = \boldsymbol{P}_j \boldsymbol{A}_{j-1,n+1} - \boldsymbol{Q}_j \boldsymbol{\phi}_{j-1,n+1} + \boldsymbol{R}_j \tilde{\boldsymbol{\phi}}_{j+1,n+1} - \boldsymbol{C}_j \tilde{\boldsymbol{V}}_{j,n+1} \quad , \quad j = 1, \ldots, J-1 \tag{86}$$

Correction:

$$\boldsymbol{d}_{n+1} = \tilde{\boldsymbol{d}}_{n+1} + \beta \Delta t^2 \boldsymbol{a}_{n+1} \tag{87}$$

$$\boldsymbol{v}_{n+1} = \tilde{\boldsymbol{v}}_{n+1} + \gamma \Delta t \boldsymbol{a}_{n+1} \tag{88}$$

$$\boldsymbol{\phi}_{j,n+1} = \tilde{\boldsymbol{\phi}}_{j,n+1} + \beta \Delta t^2 \boldsymbol{A}_{j,n+1} \quad , \quad j = 1, \ldots, J-1 \tag{89}$$

$$\boldsymbol{V}_{j,n+1} = \tilde{\boldsymbol{V}}_{j,n+1} + \gamma \Delta t \boldsymbol{A}_{j,n+1} \quad , \quad j = 1, \ldots, J-1 \tag{90}$$

Note the order in which these calculations should be done in each time step. First, the prediction phase is performed to yield $\tilde{\boldsymbol{d}}_{n+1}$ and $\tilde{\boldsymbol{v}}_{n+1}$, as well as $\tilde{\boldsymbol{\phi}}_{j,n+1}$ and $\tilde{\boldsymbol{V}}_{j,n+1}$ for all the j's. Then (85) is solved for $\boldsymbol{a}_{n+1}$. Then $\boldsymbol{d}_{n+1}$ and $\boldsymbol{v}_{n+1}$ are calculated in the correction phase. Then (86) is solved with $j = 1$, for $\boldsymbol{A}_{1,n+1}$. Note that this equation involves on the right side $\boldsymbol{A}_{0,n+1}$ and $\boldsymbol{\phi}_{0,n+1}$, namely $\boldsymbol{a}_{n+1}$ and $\boldsymbol{d}_{n+1}$, which have already been computed.

Then $\boldsymbol{\phi}_{1,n+1}$ and $\boldsymbol{V}_{1,n+1}$ are calculated in the correction phase. Then (86) is solved with $j = 2$, for $\boldsymbol{A}_{2,n+1}$, using on the right side the vectors $\boldsymbol{A}_{1,n+1}$ and $\boldsymbol{\phi}_{1,n+1}$ which are already known. The procedure goes on in this fashion.

In (85) and (86), the predicted vector $\tilde{\boldsymbol{\phi}}_{j+1,n+1}$ has been used rather than $\boldsymbol{\phi}_{j+1,n+1}$, since the latter is not known when solving for $\boldsymbol{a}_{n+1}$ or $\boldsymbol{A}_{j,n+1}$. This may lead to a numerical instability or to poor accuracy. To avoid these, the whole solution process given by eqs. (85)–(90) is repeated, within a time step, a number of times in an iterative manner. Each additional cycle consists in solving (85) again (followed by correction), and then solving (86) (followed by correction) for $j = 1, \ldots, J-1$, while in each case using the last computed $\boldsymbol{\phi}_{j+1,n+1}$ instead of $\tilde{\boldsymbol{\phi}}_{j+1,n+1}$. Numerical experiments show that usually one additional cycle is needed to yield stable and accurate results.

6. Computational Issues

6.1. Choosing the Parameters C_j

The new Jth-order NRBC (25)–(28), like the original Higdon NRBC, involves the J parameters $C_1, \ldots, C_J$. Now the choice of these parameters is discussed.

First, it should be noted that some physical limitations may apply to the chosen values of the C_j's. In the wave-guide model considered here, one has from (9) and (10)

$$C_x = C_0 \sqrt{1 + \frac{n^2\pi^2/b^2 + f^2}{k^2}} \qquad , \qquad n = 0, 1, 2, \ldots \tag{91}$$

and thus $C_x \geq C_0$. Hence in this case one should take $C_j \geq C_0$ for all the j's.

Second, recall that even the simple choice $C_j = C_0$ for $j = 1, \ldots, J$ is guaranteed to reduce the spurious reflection as J increases (see Section 3.1). This choice may be successful in many cases provided that J is sufficiently large. What one gains from making a specialized choice for the C_j is the ability to obtain the desired level of accuracy with a smaller order J.

Third, there are three general approaches for choosing the parameters C_j:

(a) The user chooses the C_j a-priori in a manual manner based on an "educated guess."

(b) The C_j are chosen automatically by the computer code as a preprocess.

(c) The C_j are not constant, but are determined adaptively by the computer code.

Approach (a) is the one adopted by Higdon [43], and is based on the assumption that the user has some *a priori* knowledge on the character of the exact solution. While this may be a good assumption in some applications, it is definitely desirable to have at hand an automatic procedure that will not require the user's intervention.

Approach (b) is attractive since it is automatic yet very inexpensive computationally. This approach has been adopted in [44] as well as here, using an algorithm which is based on the *maximum resolvable* wave numbers in the x and y directions, and on the minimax formula [47] for choosing the x-component wave numbers. See [44] for more details.

Approach (c) is the most sophisticated, and also the most expensive computationally. In this approach, the values C_j are estimated for every node on the boundary at each time step, from the solution in the previous time-steps. For the Sommerfeld-like NRBC ($J = 1$), a procedure of this type is used a lot in meteorological applications; see [42] and references therein. Analogous procedures may be employed with higher orders. An adaptive scheme of a different type, perhaps more suitable to high orders, is based on the Fast Fourier Transform (FFT); see [48].

6.2. Computational Effort as a Function of J

It is easy to see that the number of operations related directly to the Jth-order NRBC on $\mathcal{B}$ is $O(JN_{\mathcal{B}})$ per time-step, namely increases *linearly* with the order J of the NRBC. The associated computational effort is typically marginal with respect to the total effort required by the entire solution process. In comparison, the scheme proposed in [44] which directly uses the original Higdon NRBCs (but with a special high-order finite difference discretization scheme) requires $O(3^J N_{\mathcal{B}})$ operations per time-step, namely its complexity grows *exponentially* with J.

6.3. Choice of FE Shape Functions

The FE formulation presented above allows, at least in theory, a general choice of the shape functions, namely different shape functions $N_a^{(j)}$ may be chosen for the different variables

ϕ_j. However, it is advantageous to choose all the shape functions to be the same for all the variables, for the following reasons:

1. This is convenient from the programming point of view: only one family of shape functions has to be coded.

2. This allows the use of the simplest possible interpolation, i.e., linear, for all the variables.

3. This choice makes *all* the square global matrices in (64) and (65) symmetric. See Section 4.2.

4. Moreover, it can be proved that this choice makes *all* the square global matrices in (64) and (65) positive definite or negative definite (depending on the sign of the coefficient appearing in the expressions (72)–(80)), and hence non-singular.

5. This choice, together with the assumption that the coefficients are constant in each element, makes the element matrices $\boldsymbol{c}^e$, $\boldsymbol{c}_j^e$, $\boldsymbol{p}_j^e$ and $\boldsymbol{r}_j^e$ (see (75), (77), (78) and (80)) as well as the non-zero square block of $\boldsymbol{g}^e$ (see (76)) all equal up to a constant factor, and thus enables a very efficient calculation on the element level.

However, one has to be careful with the choice of the shape functions in a mixed FE formulation like the present one, since the FE scheme must satisfy the Babuška-Brezzi (BB) condition of stability [46]. Fortunately, numerical experiments show that equal-order interpolation, and in particular bilinear shape functions in Ω for u and linear one-dimensional shape functions on $\mathcal{B}$ for all the ϕ_j, is a stable combination. No locking or other convergence difficulties have been observed. The situation is somewhat similar to the mixed FE formulation devised in [24] for time-harmonic waves. Yet, the satisfaction of the BB condition is still to be proved mathematically.

6.4. Shape of the Artificial Boundary

In the wave-guide problem considered here the artificial boundary $\mathcal{B}$ is simply a straight segment. The extension to a three-dimensional wave guide where $\mathcal{B}$ is a planar surface

is immediate. Some complication occurs when the problem under consideration is that of exterior scattering (see Fig. 1(a)), where $\mathcal{B}$ is a closed line or a closed surface. If $\mathcal{B}$ is a rectangle or a rectangular box, then it has *corners* which must be dealt with. For the well-posedness of the problem in Ω with the NRBC (25)–(28) on $\mathcal{B}$, corner conditions which relate the tangential and normal derivatives on two sides meeting at a corner must be applied. Discussion of these corner conditions is outside the scope of the present paper. If $\mathcal{B}$ has a smooth shape (e.g., a circle in two dimensions or a sphere in three dimensions) the NRBC can be adapted to this geometry by using variable transformation; see e.g. [48]. These issues are left for future research.

7. Numerical Experiments

The new FE scheme is now applied to a number of simple model problems. In each case, the FE solution is compared to a reference solution, which is *exact* as far as the boundary-condition treatment is concerned. The latter solution is obtained by solving the problem in a computational domain which is very long in the x direction. During the simulation time the wave generated on or near Γ_W does not reach the remote (east) boundary of this long domain. Thus in the reference solution the issue of spurious reflection is avoided altogether, regardless of the boundary condition used on the remote boundary. In the following figures, this reference solution will be termed 'exact' or $u_{\rm ex}$.

A uniform wave guide is considered (see Fig. 1(b)), with width $b = 3$ and medium wave speed $C_0 = 1$. There are no wave sources ($S = 0$), and on the west boundary $u = u_W = 0$ is prescribed. First $f = 0$ is taken, which corresponds to the case of a non-dispersive medium. One should note, however, that *geometrical dispersion*, which is generated by the effect of waves bouncing from the south and north walls, always occurs in wave guides, even when $f = 0$. This may be seen from the dispersion relation (10), by noting the way in which $(C_0 n\pi/b)^2$, i.e., the geometrical dispersion, is added to f^2, i.e., the medium dispersion. The initial values (see (5)) are zero everywhere except in the strip $0 \le x \le 1$. In this strip,

$$u(x, y, 0) = H_{(0,1)}(x)\ \cos\left(\frac{4\pi y}{b}\right)\ , \qquad \dot{u}(x, y, 0) = 0\ . \tag{92}$$

Here $H_{(0,1)}(x)$ is the "hat function" which varies piecewise-linearly from the value 0 at $x = 0$ to 1 at $x = 0.5$ and then to 0 again at $x = 1$.

The artificial boundary $\mathcal{B}$ is introduced at $x = x_{\mathcal{B}} = 3$. Thus, the computational domain Ω is a 3×3 square. In Ω a mesh of $60 \times 60 = 3600$ four-node square elements is employed. Equal-order interpolation is used for all the variables: bilinear shape functions for u, and linear shape functions on $\mathcal{B}$ for the ϕ_j's. For the 'exact' solution, a 9×3 rectangle is used as the computational domain, with a mesh of 180×60 elements. For the time integration, the Newmark scheme (81)–(90) is used with parameters $\beta = 0.25$ and $\gamma = 0.5$ (trapezoidal: implicit, 2nd-order accurate, unconditionally stable [46]), with a step-size $\Delta t = 0.01$.

The NRBC parameters C_j are chosen automatically by using the scheme devised in [44] (see Section 6.1). Table 1 gives the values of the C_j for $J = 1, \ldots, 4$, along with the corresponding values of the β_j and α_j which appear in the scheme (see (25)–(27), (75), (77) and (78)).

J	C_1	C_2	C_3	C_4	β_0	β_1	β_2	β_3	α_1	α_2	α_3
1	1.00				1.00						
2	1.00	1.73			0.58	1.58			-0.67		
3	1.00	1.47	2.80		0.68	1.04	1.36		-0.54	-0.87	
4	1.00	1.44	1.73	3.99	0.69	1.27	0.83	1.25	-0.52	-0.67	-0.94

Table 1. The non-dispersive wave-guide problem: values of the parameters C_j and the corresponding values of β_j and α_j.

Fig. 2 compares the 'exact' solution to the FE solutions obtained with different values of the NRBC order J. The solutions are shown along $\mathcal{B}$, at time $t = 8$. The NRBC '$J = 0$' is the zero Neumann boundary condition $\partial u/\partial x = 0$ on $\mathcal{B}$. The latter condition actually generates total reflection and hence yields huge errors, as the figure shows. The solutions corresponding to $J = 1, \ldots, 4$ approach the 'exact' solution as J is increased. The $J = 4$ solution is indistinguishable from the 'exact' solution.

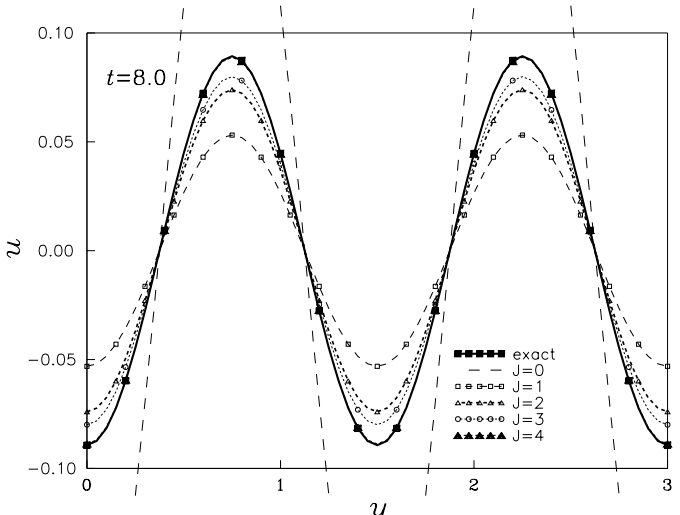

Figure 2. The non-dispersive wave-guide problem: comparison of solutions along the artificial boundary $\mathcal{B}$, at time $t = 8$.

To measure the global error, the error measure

$$E_{\mathcal{B}}(t) = \sqrt{\sum_{m=1}^{N_{\mathcal{B}}} \left(u(x_{\mathcal{B}}, y_m, t) - u_{\text{ex}}(x_{\mathcal{B}}, y_m, t)\right)^2} \tag{93}$$

is defined. This is the Eulerian norm of the error over $\mathcal{B}$. Fig. 3 shows the evolution of this error norm in time, in a logarithmic scale, for different values of J. In this figure, the values of $E_{\mathcal{B}}$ were calculated at times $t = 1, 2, \ldots, 10$ and were connected by straight lines. The global error initially increases in time, but quickly levels off. The error generally decreases with increasing J. Up to $J = 3$ the improvement achieved by increasing J is dramatic, but the errors associated with $J = 3$ and $J = 4$ are comparable. The latter fact shows that for $J \geq 3$ the dominant error is the FE discretization error and not the NRBC error.

Now the previous experiment is repeated for the *dispersive case*: the dispersion parameter is set to $f = 1$. All the other parameters remain unchanged. Fig. 4 shows the 'exact' solution and solutions obtained with $J = 0, \ldots, 4$ along $\mathcal{B}$ at time $t = 6$. As seen by comparing Figs. 2 and 4, the $J = 0$ and $J = 1$ solutions are as inaccurate as in the non-dispersive case, while again the $J = 4$ solution practically coincides with the 'exact' solution. However, interestingly, the $J = 2$ and $J = 3$ solutions are now much closer to the 'exact' solution compared to the non-dispersive case. Fig. 5 shows the global error $E_{\mathcal{B}}$ as a function of

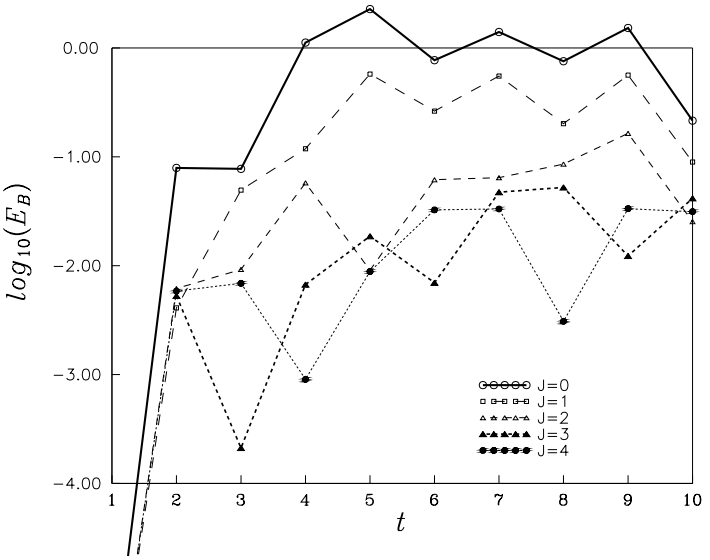

Figure 3. The non-dispersive wave-guide problem: global error $E_{\mathcal{B}}$ as a function of time for different values of the NRBC order J.

time for $J = 0, 1, \ldots 5$. Here the values at $t = 0.1,\, 0.2, \ldots, 8.0$ were plotted and connected with straight lines. The errors appear to be oscillatory and to decrease with increasing J. Again, the errors for $J \geq 3$ are comparable, which indicates that the FE discretization error dominates for these high-order NRBCs. Nevertheless, integration of the error in time shows that the $J = 4$ solution is slightly more accurate on average than the $J = 3$ solution, and that the $J = 5$ is still slightly better. (See next example for quantitative results in this context).

To demonstrate the difficulties involved in this example, we consider the angle of incidence θ of the incoming wave at the point $P(3, 1.6)$ on $\mathcal{B}$. This is defined as the angle between the wave direction γ and the normal to $\mathcal{B}$ at P, namely $\theta = |90^\circ - \gamma|$. The wave direction γ is computed via

$$\cos\gamma = \frac{\boldsymbol{\nabla} u}{|\boldsymbol{\nabla} u|} \cdot \boldsymbol{e}_y = \frac{\frac{\partial u}{\partial y}}{\sqrt{(\frac{\partial u}{\partial x})^2 + (\frac{\partial u}{\partial y})^2}} \;, \tag{94}$$

where γ is measured clockwise from the $-y$ axis and $\boldsymbol{e}_y$ is the unit vector pointing in the y direction. The partial derivatives appearing in (94) can be calculated via the expressions

$$\partial_x u = -k\ \cos\left(\frac{4\pi y}{b}\right) \sin k(x - C_x t) \;, \qquad \partial_y u = -(4\pi/b)\ \sin\left(\frac{4\pi y}{b}\right) \cos k(x - C_x t) \;, \tag{95}$$

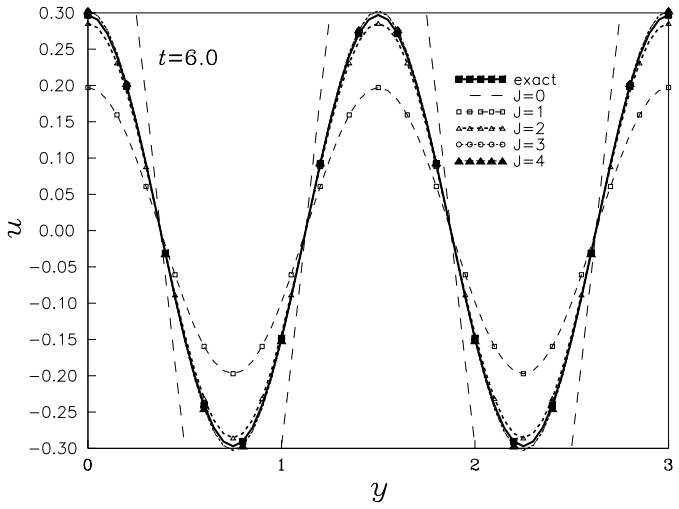

Figure 4. The dispersive wave-guide problem: comparison of solutions along the artificial boundary $\mathcal{B}$, at time $t = 6$.

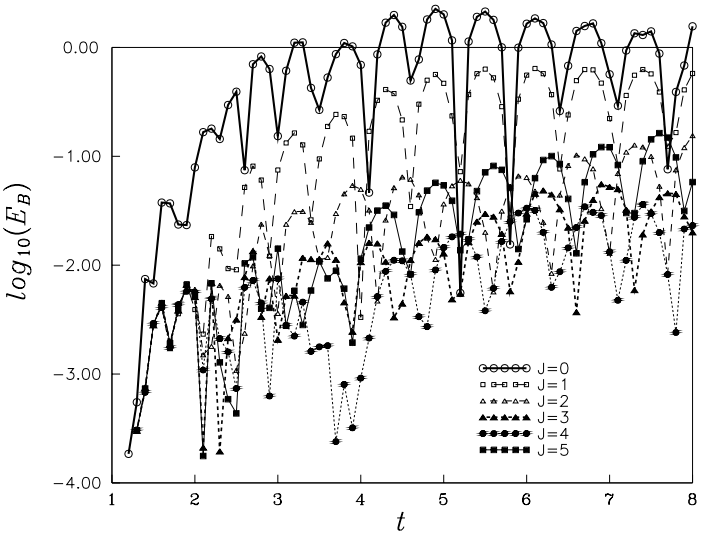

Figure 5. The dispersive wave-guide problem: global error $E_{\mathcal{B}}$ as a function of time for different values of the NRBC order J.

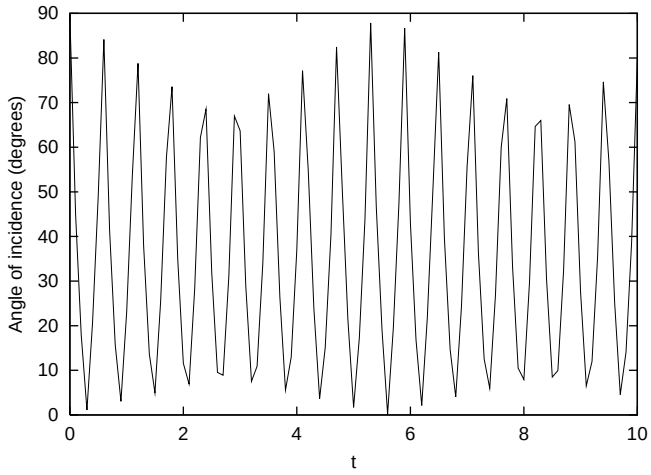

Figure 6. The dispersive wave-guide problem: angle of incidence of the incoming wave at the point $P(3, 1.6)$ on the artificial boundary $\mathcal{B}$ as a function of time.

which correspond to the mode-4 wave

$$u = \cos\left(\frac{4\pi y}{b}\right)\cos k(x - C_x t) \ . \tag{96}$$

While (96) is certainly not the exact solution of the present problem (see the initial condition (92)), the most dominant wave in the solution will have this form. We take $k = \pi$ since the "hat-function" initial condition is similar to a half sine-wave with half-period 1. Fig. 6 shows the angle of incidence θ at P as a function of time. It is seen that θ varies between 0 and 90° in an oscillatory manner. Such cases where there are waves with a wide range of incidence angles are known to be relatively difficult for NRBC treatment.

Now the wave-guide problem illustrated in Fig. 7 is considered. This problem is similar to the previous one (the dispersion parameter remains $f = 1$), with the following two differences. First, the initial conditions are zero everywhere except in the strip $0 \le x \le 1$ where

$$u(x, y, 0) = H_{(0,1)}(x) \ , \qquad \dot{u}(x, y, 0) = 0 \ . \tag{97}$$

Note that in contrast to the previous example (see (92)), the initial values do not depend on y, but only on x through the "hat function" $H_{(0,1)}(x)$. Second, the medium wave speed C_0 is not constant in Ω. It is $C_0 = 1$ everywhere except in a small square area, of size 0.2×0.2,

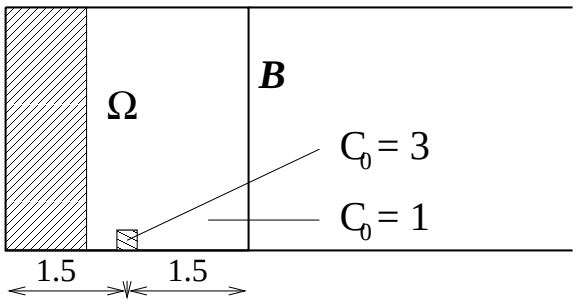

Figure 7. Setup for the 'bump' wave-guide problem.

where $C_0 = 3$. This area, shown in Fig. 7, models a 'hard bump' in the medium, which causes wave scattering inside the wave guide, and is solely responsible for the y-dependence of the solution. The 'bump' area includes 16 FEs.

Figs. 8(a) and 8(b) show the 'exact' solutions as well as solutions obtained for various values of J, along $\mathcal{B}$ at times $t = 4$ and $t = 8$, respectively. The current problem is hard enough so that even with high-order NRBCs some small error is noticeable. In particular, note that at time $t = 8$ (Fig. 8(b)), the $J = 4$ and $J = 5$ solutions almost coincide, but are slightly off the 'exact' solution. Still, they are much more accurate than the solutions corresponding to $J \leq 3$.

For a given simulation time T, one can define the global error-measure in space and time,

$$\bar{E}_{\mathcal{B}}(T) = \left(\int_0^T E_{\mathcal{B}}^2(t)\, dt \right)^{\frac{1}{2}} . \tag{98}$$

This is the accumulated error on $\mathcal{B}$ during the entire simulation. Fig. 9 shows this error as a function of the simulation time T for various values of J. For all J's, The error increases initially with the simulation time, but then become almost constant for long simulations. Unlike the instantaneous error shown in the previous figures, the accumulated error decreases monotonically with increasing J. The superiority of the $J = 5$ solution over all lower-order solutions is apparent.

Incidentally, the 'bump' problem turned out to be hard also in terms of numerical stability. In this example, two Newmark cycles (see Section 5) were not sufficient to stabilize the solution, and a third one was needed. In fact, the corners of the 'bump' area are points of sin-

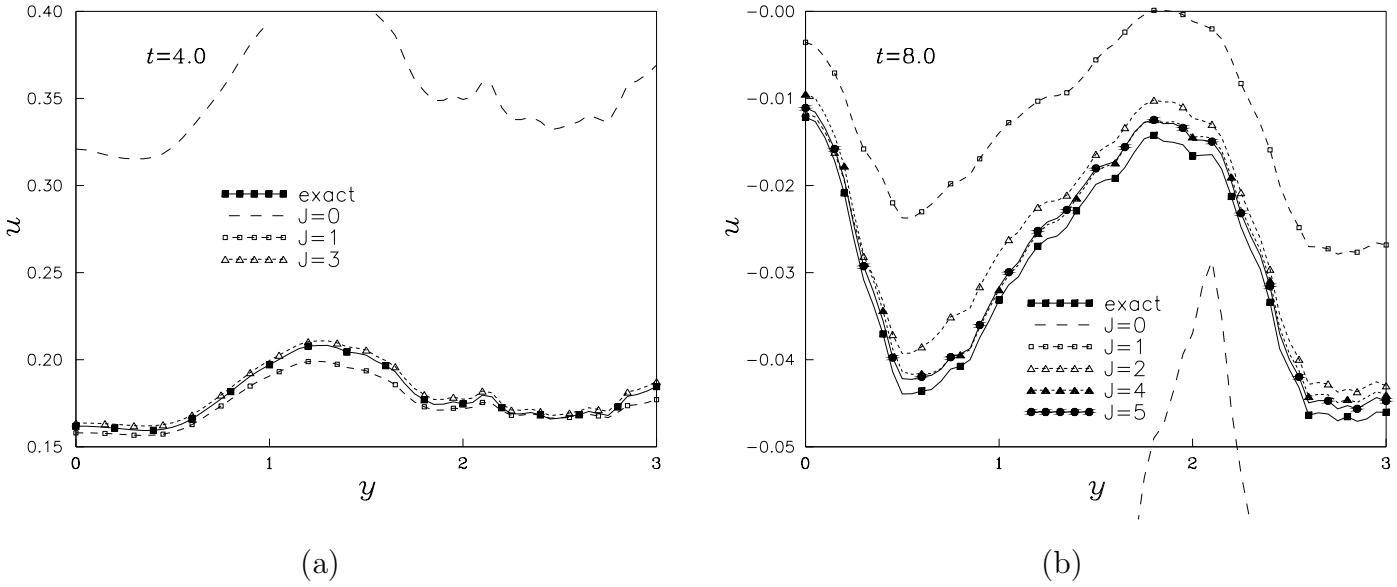

(a) (b)

Figure 8. The 'bump' wave-guide problem: comparison of solutions along the artificial boundary $\mathcal{B}$, at times (a) $t = 4$, (b) $t = 8$.

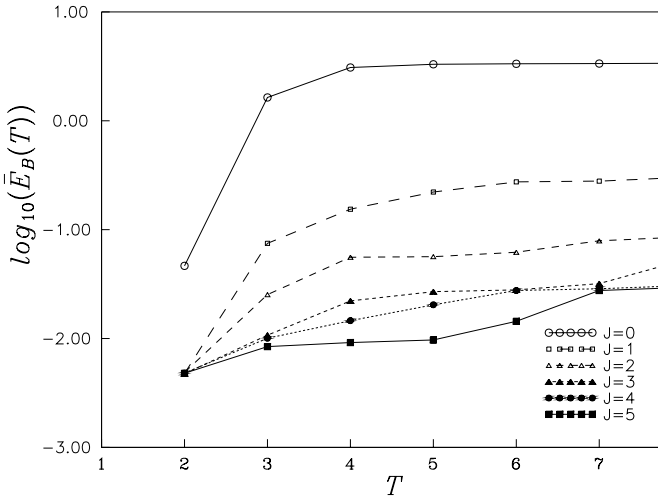

Figure 9. The 'bump' wave-guide problem: the global accumulated error $\bar{E}_{\mathcal{B}}(T)$ as a function of the simulation time T for various values of J.

gularity in the solution, which are obviously not well-resolved with the mesh and type of FEs used. However, this issue does not concern us in the present study of NRBC performance.

As a final numerical experiment, a uniform wave guide is considered again, with width $b = 5$ and medium wave speed $C_0 = 1$, and with no dispersion ($f = 0$). The initial values are zero everywhere, and the boundary function u_W on Γ_W is given by

$$u_W(y,t) = \begin{cases} \cos\left[\frac{\pi}{2r}(y - y_0)\right] & \text{if } |y - y_0| \le r \quad \& \quad 0 \ge t \le t_0 \ , \\ \\ 0 & \text{otherwise} \ . \end{cases} \tag{99}$$

Thus, the wave source on the west boundary is a cosine function in y with three parameters: its center location y_0, its width r, and its time duration t_0. The chosen parameter values are $y_0 = 2.5$, $r = 1.5$, and $t_0 = 0.5$.

The artificial boundary $\mathcal{B}$ is introduced at $x = x_{\mathcal{B}} = 5$, thus defining as the computational domain Ω a 5×5 square. In Ω a mesh of $20 \times 20 = 400$ four-node square elements is used, with linear-order interpolation for all the variables, as before. The long domain for the 'exact' solution is a 15×5 rectangle, with a mesh of 60×20 elements. As before, the Newmark scheme is used for the time-integration with the trapezoidal parameters $\beta = 0.25$ and $\gamma = 0.5$, and $\Delta t = 0.01$.

The NRBC with $J = 4$ is chosen, with parameters C_j which are obtained automatically as before. These turn out to be $C_j/C_0 = 1$, 1.44, 1.73 and 3.99. The numerical solution is compared to the 'exact' solution obtained by using the long mesh, as well as to a solution obtained in the short domain Ω but with the $J = 1$ NRBC on $\mathcal{B}$. In the latter case, the parameter $C_1 = 2.5$ is used, which is in the middle of the range of the four C_j's mentioned above.

Fig. 10(a)–(d) show the three solutions at times $t = 4$, 5, 8 and 10. In each of these figures, the top plot is that of the 'exact' solution, the middle plot corresponds to the $J = 4$ solution, and the lower plot describes the $J = 1$ solution. Both the colors and the contour lines represent values of u. At time $t = 4$ (Fig. 10(a)) the main bulk of the wave packet generated on Γ_W just reaches $\mathcal{B}$. A slight spurious reflection can be observed in the $J = 1$ solution, but overall the three solutions are very similar. The front of the wave packet crosses the boundary $\mathcal{B}$ and advances beyond it at time $t = 5$ (Fig. 10(b)). At this time, the $J = 4$

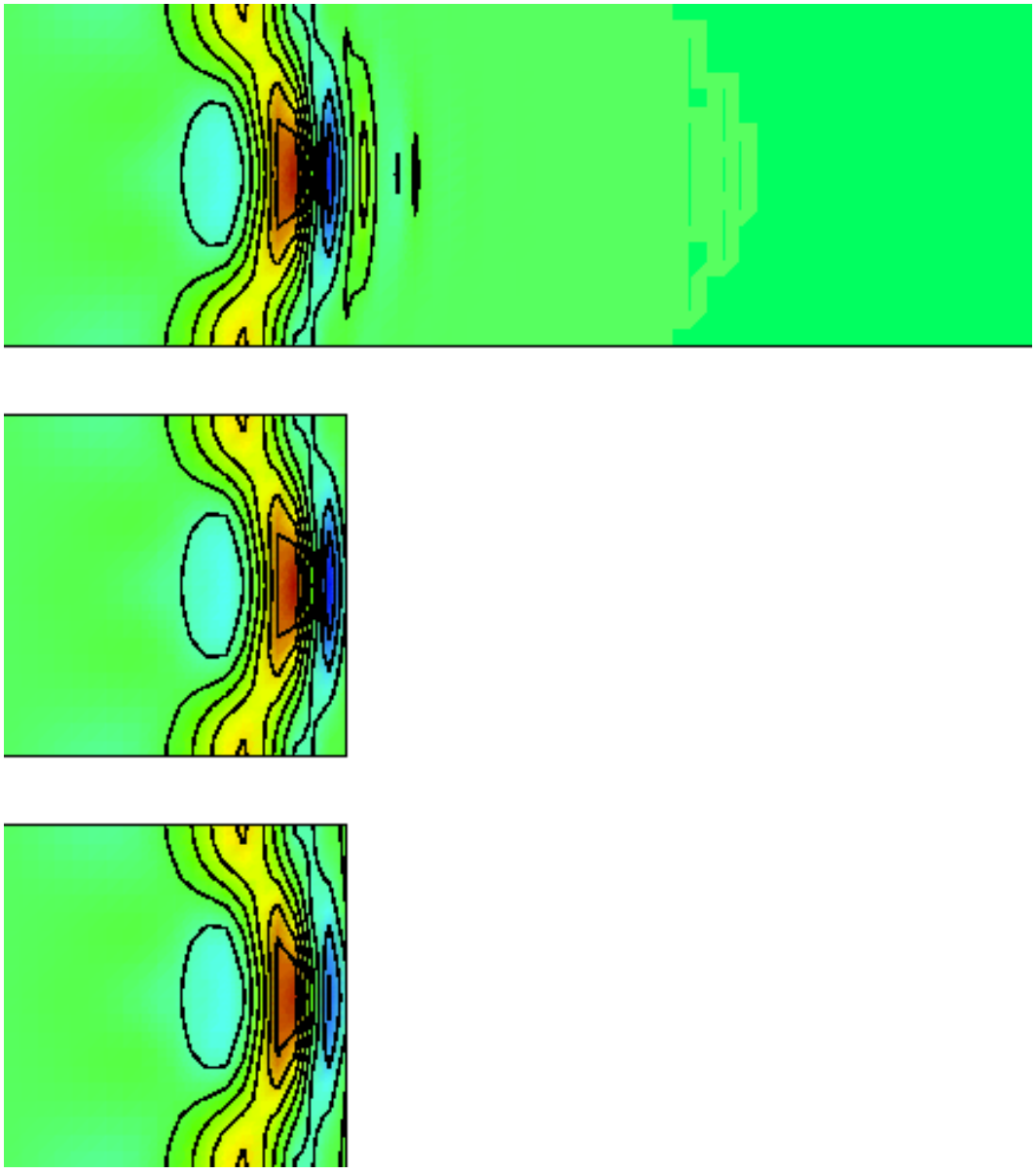

Figure 10(a)

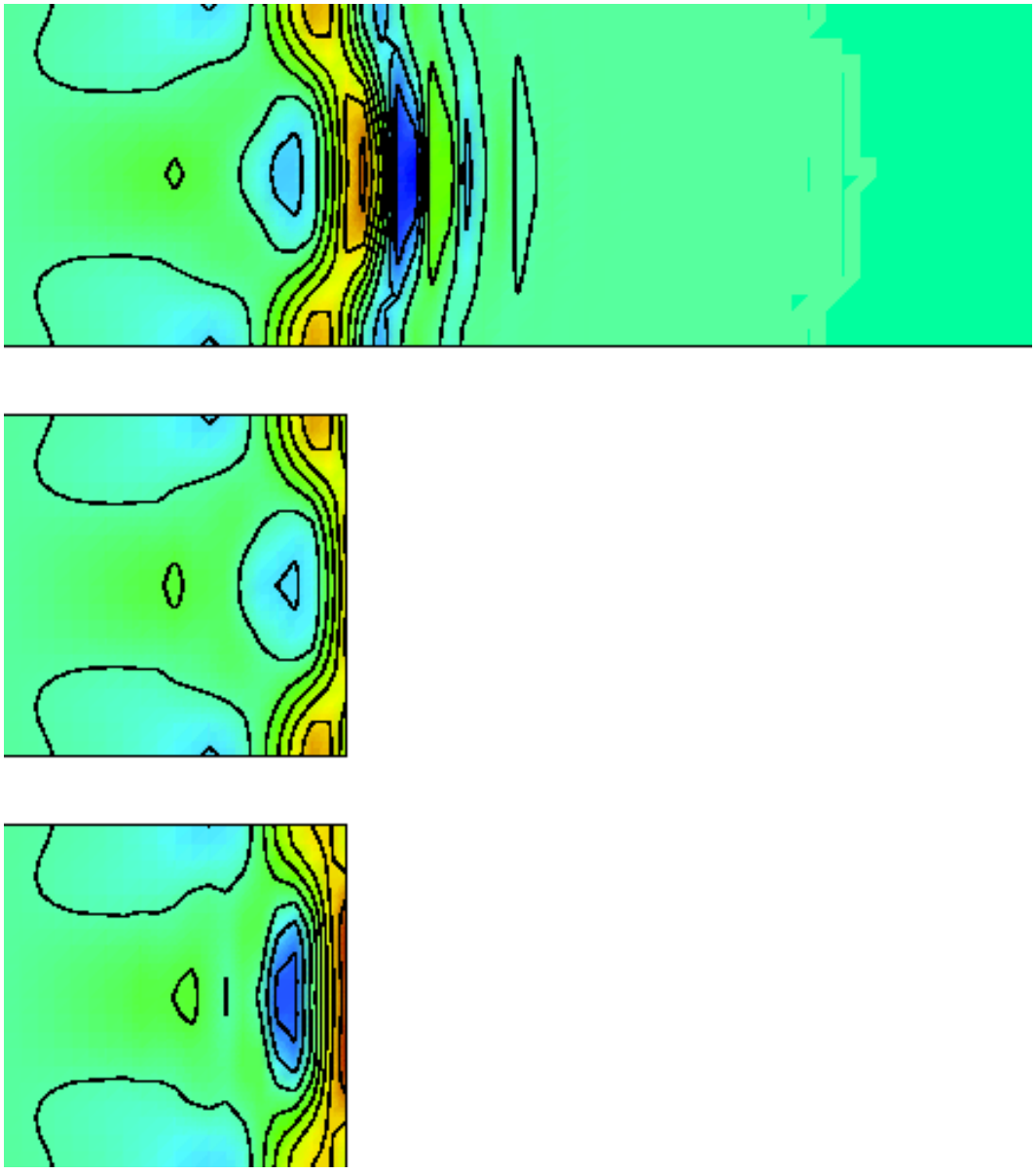

Figure 10(b)

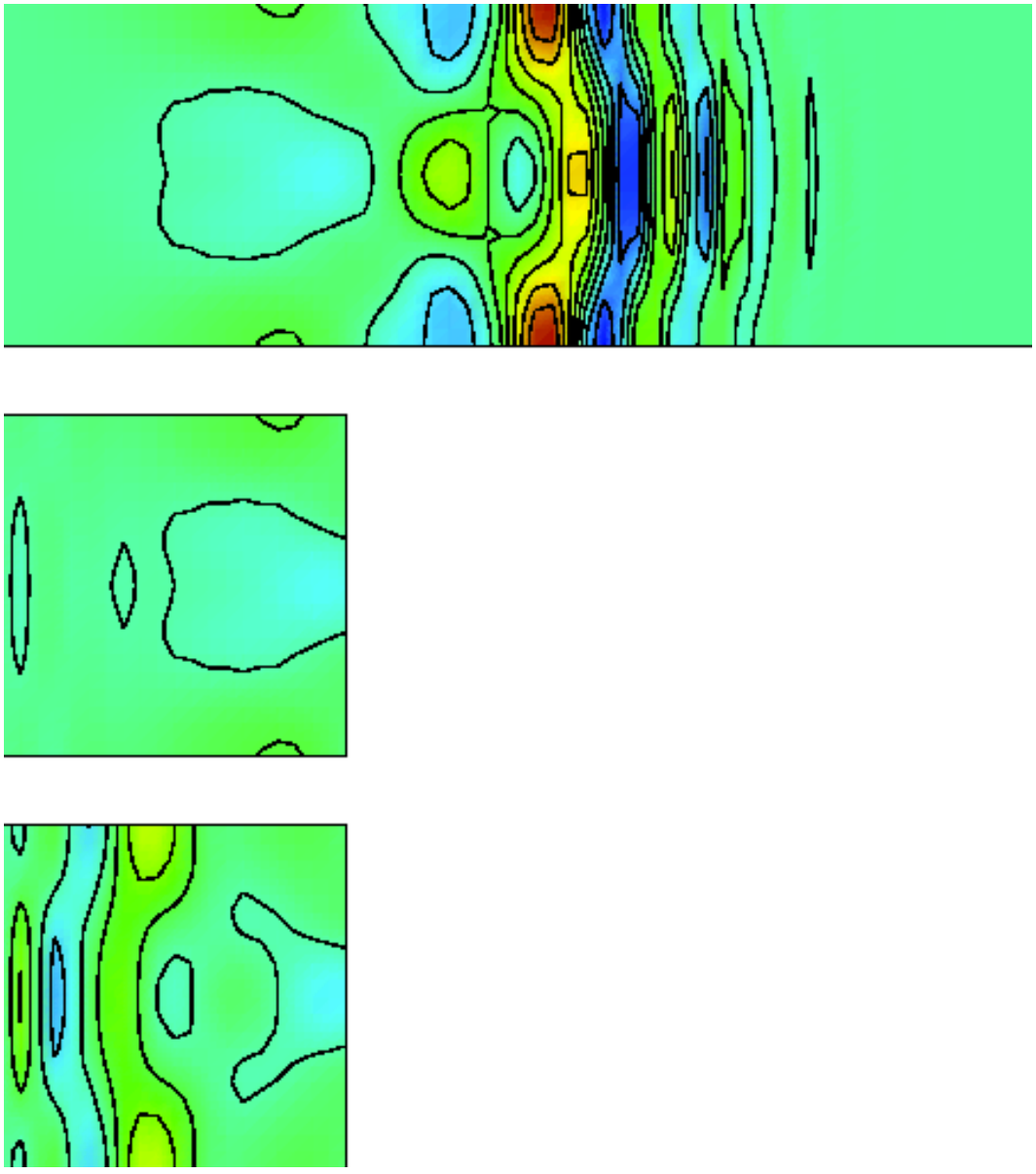

Figure 10(c)

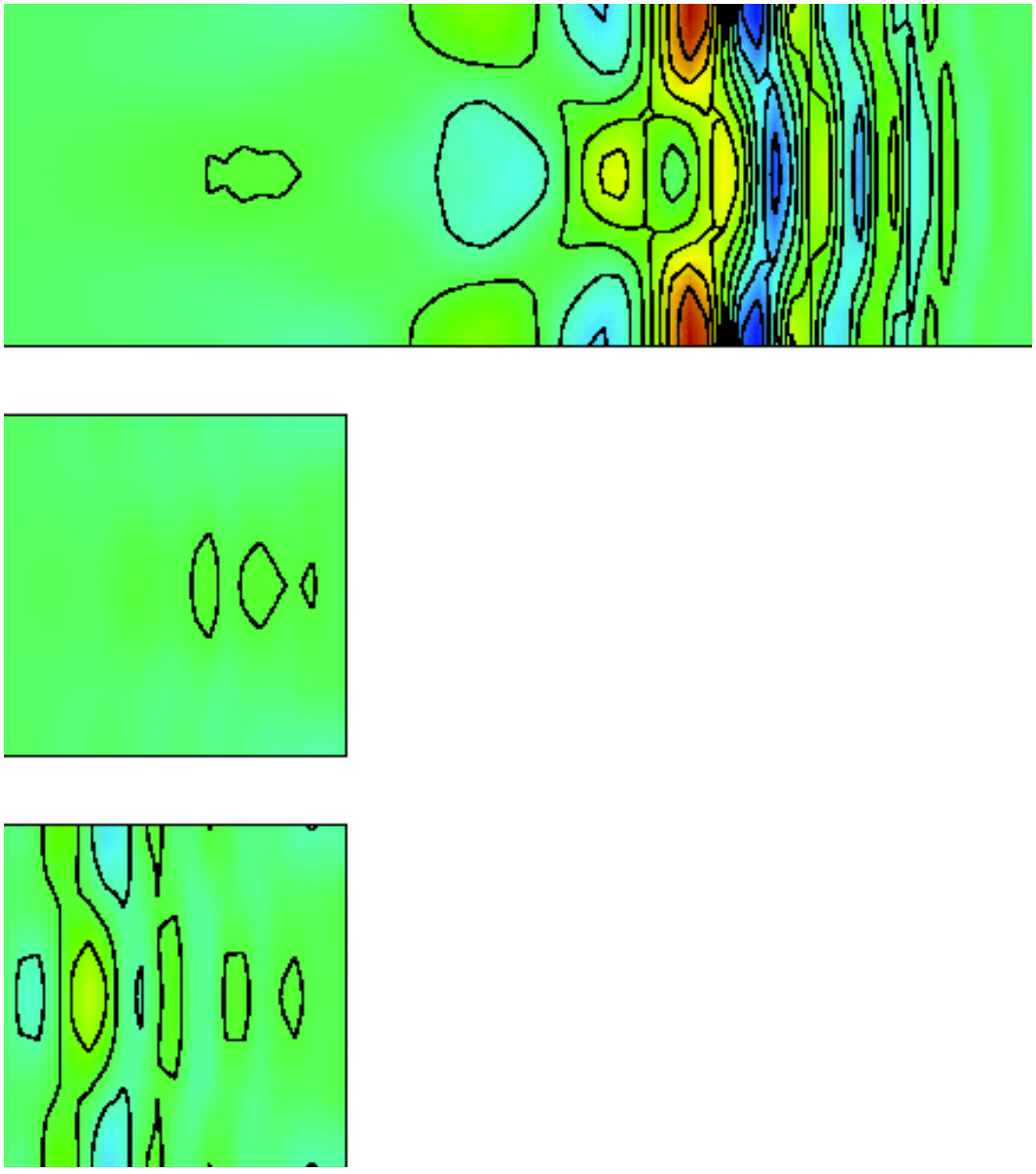

Figure 10(d)

solution is almost indistinguishable from the 'exact' solution, whereas in the $J = 1$ solution a strong spurious reflection is evident. At times $t = 8$ and 10 (Figs. 10(c) and 10(d)), most of the wave packet has left Ω. The reflected wave moves backwards in the $J = 1$ solution and pollutes the computational domain. On the other hand, the $J = 4$ solution exhibits wave traces which are similar to those present in the 'exact' solution.

In order to examine the errors generated in this example quantitatively, we introduce the global error measure $E_\Omega(t)$, defined by

$$E_\Omega(t) = \sqrt{\frac{1}{N_x N_y} \sum_{p=1}^{N_x} \sum_{q=1}^{N_y} \left(u(x_p, y_q, t) - u_{\text{ex}}(x_p, y_q, t)\right)^2} \ . \tag{100}$$

Here N_x and N_y are, respectively, the number of nodes in the x and y directions in the computational domain Ω. In traveling-pulse type problems like the present example, the error measure $E_\Omega(t)$ is preferred over $E_\mathcal{B}$ defined in (93) or $\bar{E}_\mathcal{B}$ defined in (98). The reason is that the latter measures indicate the error only over the boundary $\mathcal{B}$, while, as Figs. 7(b)–(d) demonstrate, the major errors are not necessarily found on this boundary but they penetrate the interior and constantly change their locations.

Fig. 11 shows the global error E_Ω as a function of time for the $J = 4$ solution and for the $J = 1$ solution. Up until $t = 3$, before the wave reaches the artificial boundary, both errors are extremely small. Once the wave reaches the boundary both global errors increase but the $J = 1$ error is up to 10 times larger than the $J = 4$ error.

8. Concluding Remarks

In this paper, a new FE scheme has been developed for the solution of time-dependent wave problems in unbounded domains. The FE scheme incorporates a special high-order NRBC on an artificial boundary $\mathcal{B}$ which bounds the finite computational domain. The NRBC is of an *arbitrarily high order*. The scheme is coded once and for all for any order J; J is simply an input parameter given by the user. This is enabled through the introduction of auxiliary variables on $\mathcal{B}$, which lead to a C^0 mixed FE formulation. Numerical experiments indicate that the FE scheme is stable even with equal-order interpolation, which is a very advantageous choice. Linear and bilinear shape functions for all the variables have been used

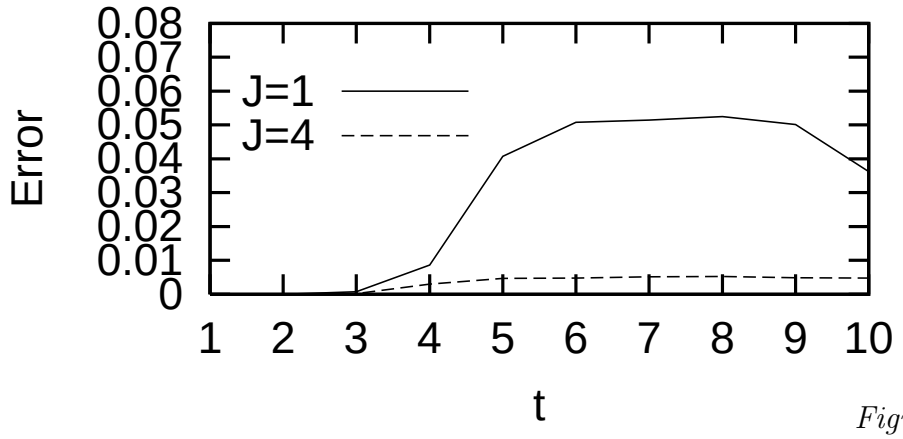

Figure 11. The west-source problem: global error E as a function of time, generated by the $J = 4$ solution and by the $J = 1$ solution.

in the numerical examples shown here, without any numerical difficulties. An automatic pre-process method of choosing the parameters appearing in the NRBC has been employed. The computational effort directly associated with the NRBC has been shown to increase only linearly with the order J.

Due to the generality of the proposed NRBCs it is possible to use them for problems in dispersive and stratified media. Good performance of the scheme has been demonstrated in both the non-dispersive and dispersive cases.

Related future work will include the adaptation of the proposed approach to more complicated configurations, such as exterior problems with a rectangular artificial boundary $\mathcal{B}$, and three-dimensional problems. In the former case, the non-trivial issue of corners has to be dealt with. In addition, the new FE scheme will be applied to the Shallow Water Equations (SWEs). These serve as an important testbed for more complicated models in meteorology [42]. It would be interesting, among other things, to test the performance of the high-order Higdon NRBCs when the *nonlinear* SWEs are used in the computational domain Ω. The new NRBCs will also be adapted to the case of curved artificial boundaries by using variable transformation.

Acknowledgments

This work was supported by the U.S. National Research Council (NRC), the Office of Naval Research (ONR), and the Naval Postgraduate School (NPS).

References

[1] D. Givoli, *Numerical Methods for Problems in Infinite Domains*, Elsevier, Amsterdam, 1992.

[2] B. Engquist and A. Majda, "Radiation Boundary Conditions for Acoustic and Elastic Calculations," *Comm. Pure Appl. Math.*, **32**, 313–357, 1979.

[3] A. Bayliss and E. Turkel, "Radiation Boundary Conditions for Wave-Like Equations," *Comm. Pure Appl. Math.*, **33**, 707–725, 1980.

[4] D. Givoli, "Non-Reflecting Boundary Conditions: A Review," *J. Comput. Phys.*, **94**, 1–29, 1991.

[5] P. Bettess, "Infinite Elements," *Int. J. Numer. Meth. Engng.*, **11**, 53–64, 1977.

[6] F.J. Rizzo, The Boundary Element Method — Some Early History: A Personal View, in *Boundary Elements in Structural Analysis*, D.E. Beskos, Ed., 1–16, ASCE, New York, 1989.

[7] J.B. Keller and D. Givoli, "Exact Non-Reflecting Boundary Conditions," *J. Comput. Phys.*, **82**, 172–192, 1989.

[8] D. Givoli and J.B. Keller, "Non-Reflecting Boundary Conditions for Elastic Waves," *Wave Motion*, **12**, 261–279, 1990.

[9] J.P. Bérenger, "A Perfectly Matched Layer for the Absorption of Electromagnetic Waves," *J. Comput. Phys.*, **114**, 185–200, 1994.

[10] D.S. Burnett, "A Three-Dimensional Acoustic Infinite Element Based on a Prolate Spheroidal Multipole Expansion," *J. Acoust. Soc. Am.*, **96**, pp. 2798–2816, 1994.

[11] R.J. Astley, "Transient Wave Envelope Elements for Wave Problems," *J. Sound Vib.*, **192**, 245–261, 1996.

[12] D. Givoli and I. Harari, Eds., Exterior Problems of Wave Propagation, Special Issue, *Comput. Meth. Appl. Mech. Engng.*, Vol. 164, Nos. 1–2, 1998.

[13] E. Turkel, Ed., *Appl. Numer. Math.*, Special Issue, Vol. 27, 1998.

[14] J. Astley, K. Gerdes, D. Givoli and I. Harari, Eds., Special Issue, *J. Comput. Acoust.*, Vol. 8, No. 1, 2000.

[15] S.V. Tsynkov, "Numerical Solution of Problems on Unbounded Domains, A Review," *Appl. Numer. Math.*, **27**, 465–532, 1998.

[16] D. Givoli, "Exact Representations on Artificial Interfaces and Applications in Mechanics," *Appl. Mech. Rev.*, **52**, 333–349, 1999.

[17] T. Hagstrom, "Radiation Boundary Conditions for the Numerical Simulation of Waves," *Acta Numerica*, **8**, 47–106, 1999.

[18] F. Collino, "High Order Absorbing Boundary Conditions for Wave Propagation Models. Straight Line Boundary and Corner Cases," in *Proc. 2nd Int. Conf. on Mathematical & Numerical Aspects of Wave Propagation*, R. Kleinman et al., Eds., SIAM, Delaware, pp. 161-171, 1993.

[19] M.J. Grote and J.B. Keller, "Nonreflecting Boundary Conditions for Time Dependent Scattering," *J. Comput. Phys.*, **127**, 52–65, 1996.

[20] I.L. Sofronov, "Conditions for Complete Transparency on the Sphere for the Three-Dimensional Wave Equation," *Russian Acad. Dci. Dokl. Math.*, **46**, 397–401, 1993.

[21] T. Hagstrom and S.I. Hariharan, "A Formulation of Asymptotic and Exact Boundary Conditions Using Local Operators," *Appl. Numer. Math.*, **27**, 403–416, 1998.

[22] M.N. Guddati and J.L. Tassoulas, "Continued-Fraction Absorbing Boundary Conditions for the Wave Equation," *J. Comput. Acoust.*, **8**, 139–156, 2000.

[23] D. Givoli, "High-Order Non-Reflecting Boundary Conditions Without High-Order Derivatives," *J. Comput. Phys.*, **170**, 849–870, 2001.

[24] D. Givoli and I. Patlashenko, "An Optimal High-Order Non-Reflecting Finite Element Scheme for Wave Scattering Problems," *Int. J. Numer. Meth. Engng.*, **53**, 2389–2411, 2002.

[25] E. Turkel and A. Yefet, "Absorbing PML Boundary Layers for Wave-Like Equations," *Appl. Numer. Math.*, **27**, 533–557, 1998.

[26] F. Collino and P. Monk, "The Perfectly Matched Layer in Curvilinear Coordinates," *SIAM J. Sci. Comp.*, **19**, 2061–2090, 1998.

[27] L. Ting and M.J. Miksis, "Exact Boundary Conditions for Scattering Problems," *J. Acoust. Soc. Am.*, **80**, 1825–1827, 1986.

[28] D. Givoli and D. Cohen, "Non-reflecting Boundary Conditions Based on Kirchhoff-type Formulae," *J. of Comput. Phys.*, **117**, 102–113. 1995.

[29] A.J. Safjan, "Highly Accurate Non-Reflecting Boundary Conditions for Finite Element Simulations of Transient Acoustics Problems," *Comput. Meth. Appl. Mech. Engng.*, **152**, 175–193, 1998.

[30] D. Givoli, "A Spatially Exact Non-Reflecting Boundary Condition for Time Dependent Problems," *Comput. Meth. Appl. Mech. Engng.*, **95**, 97–113, 1992.

[31] I. Patlashenko, D. Givoli and P. Barbone, "Time-Stepping Schemes for Systems of Volterra Integro-Differential Equations," *Comput. Meth. Appl. Mech. Engng.*, **190**, 5691–5718, 2001.

[32] L.L. Thompson and P.M. Pinsky, "Space-Time Finite Element Method for Structural Acoustics in Infinite Domains. Part 2: Exact Time-Dependent Non-Reflecting Boundary Conditions," *Comput. Meth. Appl. Mech. Engng.*, **132**, 229–258, 1996.

[33] B. Alpert, L. Greengard and T. Hagstrom, "Rapid Evaluation of Nonreflecting Boundary Kernels for Time-Domain Wave Propagation," SIAM J. Numer. Anal., **37**, 1138–1164, 2000.

[34] B. Alpert, L. Greengard and T. Hagstrom, "An Integral Evolution Formula for the Wave Equation," *J. Comput. Phys.*, **162**, 536–543, 2000.

[35] L.L. Thompson and R. Huan, "Finite Element Formulation of Exact Nonreflecting Boundary Conditions for the Time-Dependent Wave Equation," *Int. J. Numer. Meth. Engng.*, **45**, 1607–1630, 1999.

[36] R. Huan and L.L. Thompson, "Accurate Radiation Boundary Conditions for the Time-Dependent Wave Equation on Unbounded Domains," *Int. J. Numer. Meth. Engng.*, **47**, 1569–1603, 2000.

[37] S. Krenk, "Unified Formulation of Radiation Conditions for the Wave Equation," *Int. J. Numer. Meth. Engng.*, **53**, 275–295, 2002.

[38] I.M. Navon, B. Neta and M.Y. Hussaini, " A Perfectly Matched Layer Formulation for the Nonlinear Shallow Water Equations Models: The Split Equation Approach," to appear.

[39] D. Givoli, "Recent Advances in the DtN Finite Element Method for Unbounded Domains," *Archives of Comput. Meth. in Engng.*, **6**, 71–116, 1999.

[40] G.B. Whitham, *Linear and Nonlinear Waves*, Wiley, New York, 1974.

[41] J. Pedlosky, *Geophysical Fluid Dynamics*, Springer, New York, 1987.

[42] D.R. Durran, *Numerical Methods for Wave Equations in Geophysical Fluid Dynamics*, Springer, New York, 1999.

[43] R.L. Higdon, "Radiation Boundary Conditions for Dispersive Waves," *SIAM J. Numer. Anal.*, **31**, 64–100, 1994.

[44] D. Givoli and B. Neta, "High-Order Non-Reflecting Boundary Conditions for Dispersive Waves," *Wave Motion*, submitted.

[45] D. Givoli and B. Neta, "High-Order Non-Reflecting Boundary Scheme for Time-Dependent Waves," *J. Comput. Phys.*, submitted.

[46] T.J.R. Hughes, *The Finite Element Method*, Prentice Hall, Englewood Cliffs, N.J., 1987.

[47] B.P. Sommeijer, P.J. van der Houwen and B. Neta, "Symmetric Linear Multistep Methods for Second Order Differential Equations with Periodic Solutions," *Applied Numerical Mathematics*, **2**, 69–77, 1986.

[48] D. Givoli and B. Neta, "High-Order Higdon Non-Reflecting Boundary Conditions for the Shallow Water Equations," Rep. NPS-MA-02-001, Naval Postgraduate School, Monterey, CA, 2002.

Captions for Figures

Fig. 1. Setup for the NRBC method: (a) an exterior scattering problem; (b) a semi-infinite wave-guide problem.

Fig. 2. The non-dispersive wave-guide problem: comparison of solutions along the artificial boundary $\mathcal{B}$, at time $t = 8$.

Fig. 3. The non-dispersive wave-guide problem: global error $E_{\mathcal{B}}$ as a function of time for different values of the NRBC order J.

Fig. 4. The dispersive wave-guide problem: comparison of solutions along the artificial boundary $\mathcal{B}$, at time $t = 6$.

Fig. 5. The dispersive wave-guide problem: global error $E_{\mathcal{B}}$ as a function of time for different values of the NRBC order J.

Fig. 6. The dispersive wave-guide problem: angle of incidence of the incoming wave at the point $P(3, 1.6)$ on the artificial boundary $\mathcal{B}$ as a function of time.

Fig. 7. Setup for the 'bump' wave-guide problem.

Fig. 8. The 'bump' wave-guide problem: comparison of solutions along the artificial boundary $\mathcal{B}$, at times (a) $t = 4$, (b) $t = 8$.

Fig. 9. The 'bump' wave-guide problem: the global accumulated error $\bar{E}_{\mathcal{B}}(T)$ as a function of the simulation time T for various values of J.

Fig. 10. Solution of the west-source problem, with no dispersion. The top plot is the 'exact' solution, the middle plot is the $J = 4$ solution, and the lower plot is the $J = 1$ solution. Solutions are shown at times: (a) $t = 4$, (b) $t = 5$, (c) $t = 8$, (d) $t = 10$.

Fig. 11. The west-source problem: global error E as a function of time, generated by the $J = 4$ solution and by the $J = 1$ solution.